Heterogeneous Idealization of Ion Channel Recordings – Open Channel Noise

Florian Pein, Annika Bartsch, Claudia Steinem, and Axel Munk

***Abstract*— We propose a new model-free segmentation method for idealizing ion channel recordings. This method is designed to deal with heterogeneity of measurement errors. This in particular applies to open channel noise which, in general, is particularly difficult to cope with for model-free approaches. Our methodology is able to deal with lowpass filtered data which provides a further computational challenge. To this end we propose a multiresolution testing approach, combined with local deconvolution to resolve the lowpass filter. Simulations and statistical theory confirm that the proposed idealization recovers the underlying signal very accurately at presence of heterogeneous noise, even when events are shorter than the filter length. The method is compared to existing approaches in computer experiments and on real data. We find that it is the only one which allows to identify openings of the PorB porine at two different temporal scales. An implementation is available as an R package.**

***Index Terms*— Deconvolution, dynamic programming, flickering, heterogeneous noise, *m*-dependency, model-free, non-stationary noise, peak detection, planar patch clamp, PorB, robustness, statistical multiresolution criterion.**

I. Introduction

THE voltage patch clamp technique is a major tool to quantify the electrophysiological dynamics of ion channels in the cell membrane [1], [2]. It allows to record the conductance trace (i.e., the recorded current trace divided by the applied voltage) of a *single* ion channel in time, which is for instance important in medical research for the development of new drugs [3], [4]. Important channel characteristics such as amplitudes and dwell times can be obtained provided the conductance changes of the traces are *idealized* (underlying signal is reconstructed) from these recordings (data points) [2], [5]–[7]. To obtain such an idealization an extensive amount of methodology is available nowadays, a selective review is given below.

Manuscript received April 27, 2020; revised September 3, 2020; accepted October 7, 2020. Date of publication October 14, 2020; date of current version December 30, 2020. This work was supported in part by DFG (projects Z02 and A01, Cluster of excellence 2067 MBExC Multiscale Bioimaging: From Molecular Machines to Networks of Excitable Cells), under Grant CRC803, in part by the Volkswagen Foundation (FBMS), and in part by EPSRC – Statscale programme under Grant EP/N031938/1. *(Corresponding author: Florian Pein.)*

Florian Pein is with the Statistical Laboratory, Department of Pure Mathematics and Mathematical Statistics (DPMMS), University of Cambridge, Cambridge CB3 0WB, U.K. (e-mail: fp366@cam.ac.uk).

Annika Bartsch and Claudia Steinem are with the Institute of Organic and Biomolecular Chemistry, Georg-August University of Goettingen, 37077 Göttingen, Germany.

Axel Munk is with the Institute for Mathematical Stochastics, Georg-August-University of Goettingen, 37077 Göttingen, Germany, also with the Max Planck Institute for Biophysical Chemistry, 37077 Göttingen, Germany, and also with the Felix Bernstein Institute for Mathematical Statistics in the Biosciences, 37077 Göttingen, Germany.

This article has supplementary downloadable material available at https://ieeexplore.ieee.org, provided by the authors.

Digital Object Identifier 10.1109/TNB.2020.3031202

A. Open Channel Noise

In this paper, we focus on recordings that are affected by *open channel noise*, i.e., have larger noise on segments with a larger conductance. The name open channel noise refers to the fact that a larger conductance results from an open pore. The additional noise when the channel is open can for instance be explained by current interruptions lasting approximately 1 microsecond [8]–[13]. We analyze these recordings in a 'model-free' manner, i.e., without assuming a hidden Markov or related model, as a time series which is obtained by equidistant sampling from the convolution of a piecewise constant signal contaminated by white noise with the kernel of a lowpass filter. The white noise is scaled by an unknown piecewise constant standard deviation function to allow variance heterogeneity caused by open channel noise. We stress, that this modeling is rather general and also allows to deal with heterogeneity of measurement errors, not necessarily due to open channel noise. It will be explained in full detail in Section II.

B. Data: The Outer Membrane Porin PorB

Fig. 1 shows exemplarily a conductance trace of the outer membrane porin PorB from *Neisseria meningitidis*, a pathogenic bacterium in the human nose and throat region [14]. PorB is a trimeric porin and the second most abundant protein in the outer membrane of *Neisseria meningitidis*. It is for instance relevant for the transport of antibiotics into the cell and hence of current interest to understand antibiotic resistance better. Recordings are obtained by the patch clamp technique using solvent-free bilayers. In Fig. 1 it is clearly visible that the two conductance levels around 0.04 nS and 0.36 nS are affected from open channel noise as the variance of observations around 0.36 nS is much larger than of the ones around 0.04 nS. Such recordings were manually analyzed in [15] (Fig. 1 and its explanation). They have been a major motivation for our work as they show distinct heterogeneous noise but also short event times, which we could not tackle satisfactorily by existing idealization methods, but also not by

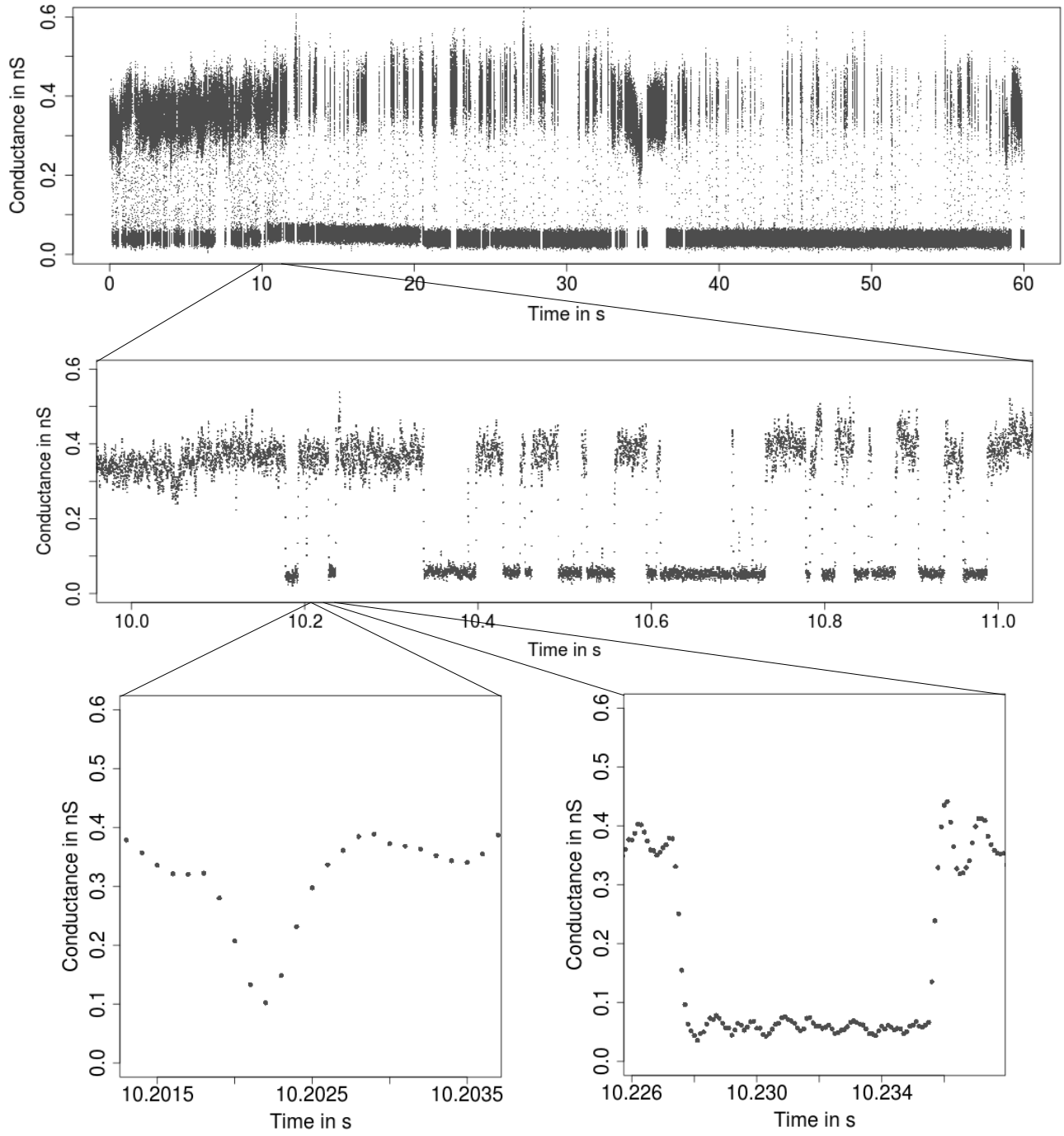

Fig. 1. From seconds to microseconds: Ion channel recordings (grey points) displayed at a level of seconds (top panel), of milliseconds (middle panel) and of microseconds (bottom panels). Data points result from a representative conductance recording of PorB by the patch clamp technique using solvent-free bilayers at 20 mV.

a manual analysis. In fact, in [15] only the conductance levels were investigated but not the full gating dynamics, since events on short time scales could not be idealized.

C. Methods for Open Channel Noise

Idealization methodology can be divided into so called model-free methods [5]–[7], [16], [17] which do not rely on a specific model for the gating dynamics, to methodology based on hidden Markov models (HMM) [18]–[23] and to current distribution fitting [13], [24]–[26]. The latter often assume a hidden Markov model as well but focus on parameter estimation directly. An idealization can be obtained by the Viterbi algorithmus [27] as soon as the parameters are determined.

Most HMM methods can deal with heterogeneous noise. Moreover, they allow to extrapolate information from larger (observable) to smaller (not observable) time scales and hence can provide a good idealization on small temporal

scales. However, they rely heavily on the correctness of the assumed model assumptions. Up to few exceptions, see [28]–[31], a Markov model is a reasonable assumption for the underlying ion channel dynamics. If valid, they offer a compact representation of the underlying processes and allow to produce traces of stochastic channel dynamics and the open and closed states can be interpreted as conformational states of the channel protein. However, artifacts in the data observed, for instance base line fluctuations, occur frequently in ion channel recordings and require elaborate data cleaning before a HMM can be fitted. Base line fluctuations are for instance caused by small defects in the membrane, which is unavoidable in the recordings. There might be also periodic oscillations, resulting from the electronics or from building vibrations (although damped). The PorB measurements display in Fig. 1 show several artifacts of this type (see for instance the waviness of the observations or the conductance increase around 10.1 s, which severely hinders straightforward fitting by a HMM: We tried to fit this data set with in total four different hidden Markov model approaches. We achieved the best results when we assumed three states, but with the assumption that two states (with small conductivity) share the same expectation and variance. More details, also on parameter choices, are given in Appendix D in the supplement. The obtained idealization is shown in Fig. 2. It fits long events well, but misses very short events, see for instance the lower left panel. Fitting such events well requires to take into account the filtering which is computationally very demanding for HMMs. We will discuss such an approach in Appendix D in the supplement as well. In summary, in addition, to the low robustness against artifacts, the choice of a specific Markov model, especially the determination of the number of states, can be a demanding task and often involves subjective choices by the analyst.

Contrary, model-free approaches can deal way more flexible with artifacts as they act rather locally on the time series without the assumption of a global model. Hence they are more robust than HMMs to model violations. Therefore, they complement HMMs well. For example, model-free methods can be used as a preprocessing step and to select or verify a specific Markov model, in particular to determine the number of states and possible transitions, as they explore and potentially remove artifacts in a model-free manner. Model-free idealizations can be used to estimate parameters of Markov models, see Sections IV-D and V-C for examples, but in comparison to HMMs further post-processing steps are required. See also [7] for a more extensive discussion of further aspects of the different approaches.

To the best of our knowledge, all existing model-free approaches assume (implicitly or explicitly) homogeneous noise and hence produce unreliable results when open channel noise is present. Among the first methods which fall into this category is TRANSIT [16]. An idealization by this approach, details of its limitations in our setting and further discussions can be found in Appendix D in the supplement. Throughout the paper we will refer to multiple multiscale model-free idealization approaches from our working group. Table I gives readers a concise reference point and an overview about their characteristics. In Fig. 3 we display JULES [7], a novel multiscale approach that also falls into this type of methods. It detects many small events on segments with a larger conductance and variance, but none on ones with a smaller conductance and variance. These additional events are most likely artifacts caused by open channel noise. Indeed, in Section IV-D we found that the rates of a simulated hidden Markov model with parameters similar to them underlying the observations in Fig. 1 could not be recovered when we used JULES to idealize the underlying signal. This effect is even more severe when the variance heterogeneity is larger.

Recently, there has been made some progress to adjust for heterogeneous noise in the context of model-free methods. However, they are not dedicated to idealize ion channel recordings, which means in particular that they do not incorporate lowpass filtering. Obviously, ignoring the filtering will deteriorate results. For illustration purposes we display the heterogeneous multiscale approach HSMUCE [33] in Fig. 4. We found that it provides reasonable results on larger temporal scales. However, due to filtering HSMUCE misses shorter events, see for instance the missed peaks around 10.2 s (lower left panel), 10.4 s or 10.7 s. Also for this type of methods we provide further examples and discussions in Appendix D in the supplement.

The occurrence of short events is often called *flickering*. Missing them does not only potentially disturb the analysis of the general channel behavior, the analysis and hence the idealization of flickering events is also of its own interest in many applications, since flickering has often its own dynamics and can result from different molecular processes. Typical examples are conformational changes of the ion channel [34] or the passage of larger molecules blocking the ions pathway through the channel [15], [35]. Hence, one main goal of this paper will be to idealize and detect such events as well.

To this end, we introduce in Section II a statistical model which resembles all features (open channel noise, events on a large range of scales, filtering) of such complex data as in the previous example. In summary, we then ask for a model-free idealization method that adapts automatically to heterogeneous noise, hence is able to detect and idealize events on a large range of relevant scales accurately, but in particular also events shorter than the filter length. Furthermore, we aim to provide theoretical justification for the detected events (controlling false positives) and for a computationally efficient method to deal with large data sets.

D. HILDE

To address these tasks, we propose in this paper a new method called **H**eterogeneous **I**dealization by **L**ocal testing and **DE**convolution, HILDE. This method combines multiscale regression and deconvolution as it takes into account the convolution of the signal with the lowpass filter explicitly for detecting events that are short in time. Before we will explain our (quite involved) methodology further, we discuss firstly the general challenges: A major difficulty for any such method due to the presence of heterogeneous noise is to distinguish between small jumps in the signal and random fluctuations caused by the noise of unknown level. However,

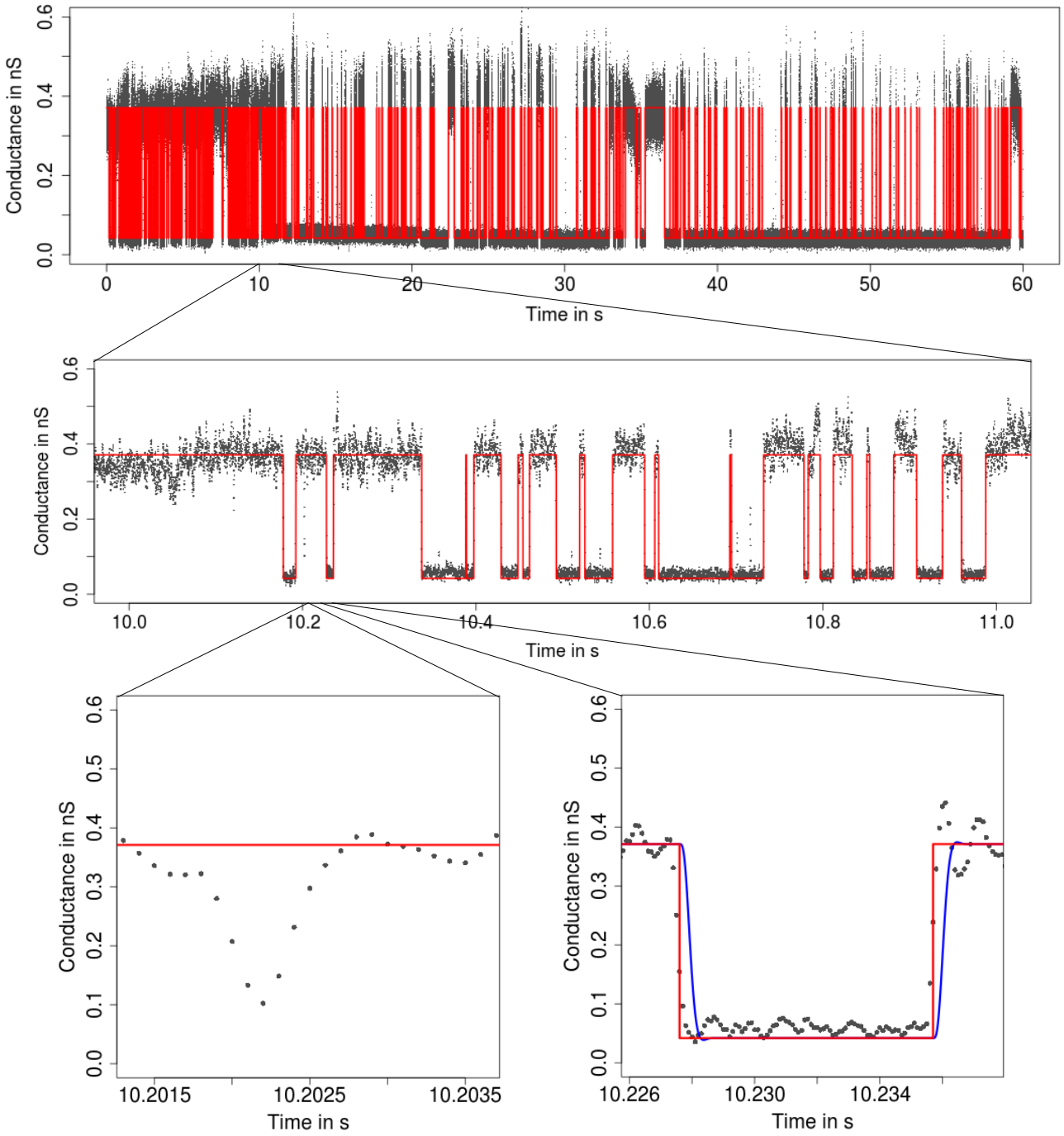

Fig. 2. Idealization (red) of the data in Figure 1 assuming a HMM displayed on three different temporal scales. The model consists of three states, whereby two states are assumed to have the same expectation and variance. In the lower panels we also show the convolution of the idealization with the lowpass filter (blue). It fits most part of the data well, but misses short events, for instance the event displayed in lower left panel.

simultaneously estimating the signal and the noise level locally is notoriously difficult in general [33] and further hampered in our situation since the unknown signal and noise are both smoothed by the filter and hence deconvolution is required when shorter temporal scales are considered. We solve this by means of a multiresolution approach in combination with a local deconvolution to idealize events on all relevant temporal scales accurately. Whereas statistical multiresolution idealization that ignores the deconvolution can be computed efficiently by dynamic programming, see for instance [6], [32], [33], combining multiresolution procedures with deconvolution is algorithmically difficult, since due to the coupling of all observations in the idealization, dynamic programming is not applicable without further ado. We will overcome this burden by focusing firstly on larger temporal scales and then improving the idealization on smaller temporal scales.

TABLE I

OVERVIEW ABOUT MULTISCALE MODEL-FREE IDEALIZATION APPROACHES. WE LIST FOR EACH METHOD WHETHER IT HAS AN OPTION TO RESTRICT TO HOMOGENEOUS NOISE, WHETHER IT ALLOWS FOR HETEROGENEOUS NOISE, WHETHER IT TAKES INTO ACCOUNT LOWPASS FILTERING AND HOW LONG AN EVENT HAS TO BE SUCH THAT IT CAN BE IDEALIZED RELIABLY. THE EXACT LENGTH DEPENDS ON THE SIGNAL TO NOISE RATION, ON FILTERING AND ON TUNING PARAMETERS, BUT IN A USUAL SETTING 'FEW TIMES' MEANS TWO TO THREE TIMES AND 'SEVERAL TIMES' MEANS AROUND FIVE TIMES, FOR FURTHER DETAILS CONFER THE REMARKS AND SIMULATIONS IN THE REFERENCED PAPERS. CONTRIBUTIONS OF THIS PAPER ARE MARKED IN BOLD. *SMUCE AND HSMUCE ARE IN PRINCIPLE ABLE TO IDEALIZE MUCH SHORTER EVENTS, BUT SINCE THEY DO NOT TAKE INTO ACCOUNT FILTERING, SUBSAMPLING IS REQUIRED TO IDEALIZE RECORDINGS WELL

Method	Homogeneous noise	Heterogeneous noise	Filtering	Minimal event length
SMUCE [32]	Yes	No	No	few times the filter length*
HSMUCE [33]	No	Yes	No	several times the filter length*
JSMURF [6]	Yes	**Yes**	Yes	few times the filter length
JULES [7]	Yes	No	Yes	few sampling points, below filter length
HILDE	**Yes**	**Yes**	**Yes**	**few sampling points, below filter length**

More precisely, HILDE consists of the following three steps: 1) detection of long events, 2) detection of short events and 3) parameter estimation by deconvolution. A summary about all three steps is given in Algorithm 1 (see Section III).

1) Detection of Long Events: We will obtain an idealization by multiresolution regression that covers all important features on larger temporal scales (for the data set analyzed here large means events with length of at least 6.5 ms, i.e., ≥ 65 sampling points). This step is discussed in Section III-B and technical details are given in Appendix A in the supplement.

2) Detection of Short Events: Our data set contains several short events that will be missed by the previous step, see for instance in Fig. 1 at around 10.2 s (lower left panel), 10.5 s, 10.7 s and 10.8 s. To detect such events, we test locally whether additional events on smaller temporal scales have to be incorporated. This is impaired by the lowpass filter and the resulting convolution has to be taken into account explicitly. To this end, we assume that signal and noise left and right of the interval on which we test are given by the idealization from the previous multiresolution step. These tests are detailed in Section III-C, while technical details are postponed to Appendix B in the supplement.

Steps a) and b) determine the number of events and their rough locations. The final idealization in Fig. 5 (see e.g. the lower left panel) confirms that step b) is indeed able to detect short events (up to 0.2 ms, corresponding to only two subsequent observations).

3) Parameter Estimation by Deconvolution: Finally, the precise locations of the events and the conductance levels have to be obtained. This will done in an additional deconvolution step, as the recordings are filtered. To this end, we use the local deconvolution approach from [7] with minor modifications. This step is discussed in Section III-D and technical details are explained in Appendix C in the supplement.

Fig. 5 shows the final idealization by HILDE of the observations in Fig. 1. Despite distinct heterogeneous noise, the idealization covers all main features on all relevant scales, in particular also short events, while at the same time it does not include systematically additional artificial changes. Zooming into single peaks (lower panels) show that HILDE fits the observations well down to a scale of microseconds, which is also a confirmation of our approach, including the modeling. We stress that HILDE is not only robust against heterogeneous noise but has typically also a larger detection power for event detection than JULES (even when the noise is homogeneous), since it takes into account the convolution explicitly for detection. This is discussed in more detail in Section VI-B, where we also outline a version of HILDE that assumes homogeneous noise to improve detection power even further if the homogeneous noise assumption is justified.

While the first and the third step are mostly useful modifications of existing methodologies, we want to stress that this is not true for the second step. To the best of our knowledge, no other model-free ion channel idealization method is able to take the convolution explicitly into account when detecting events. As discussed before, this is however indispensable to detect short events when filtering and heterogeneous noise are present.

E. Implementation and Run Time

Each step of HILDE can be computed separately. Hence, HILDE can be applied and modified in modular fashion. This allows for instance to skip the second step if a data set contains only longer events, hence saving computation time. Another usage might be to modify the local tests in the second step, for instance to increase the detection power in a data set with small conductance changes but large difference in the noise levels, without modifying the first or third step. Such modifications are discussed in Section VI-A.

The first multiresolution regression step can be computed by a pruned dynamic program. The computation of the local tests in the second step is straightforward and the deconvolution in the third step can be computed by an iterative grid search. These steps are detailed in Section III-E and summarized in Algorithm 1. An implementation is available by the function *hilde* in the `R` package *clampSeg* accompanying this paper. The package is available on request and has been submitted parallel to CRAN [36].

The worst case computational complexity is quadratic in the number of observations, but in most ion channel recordings

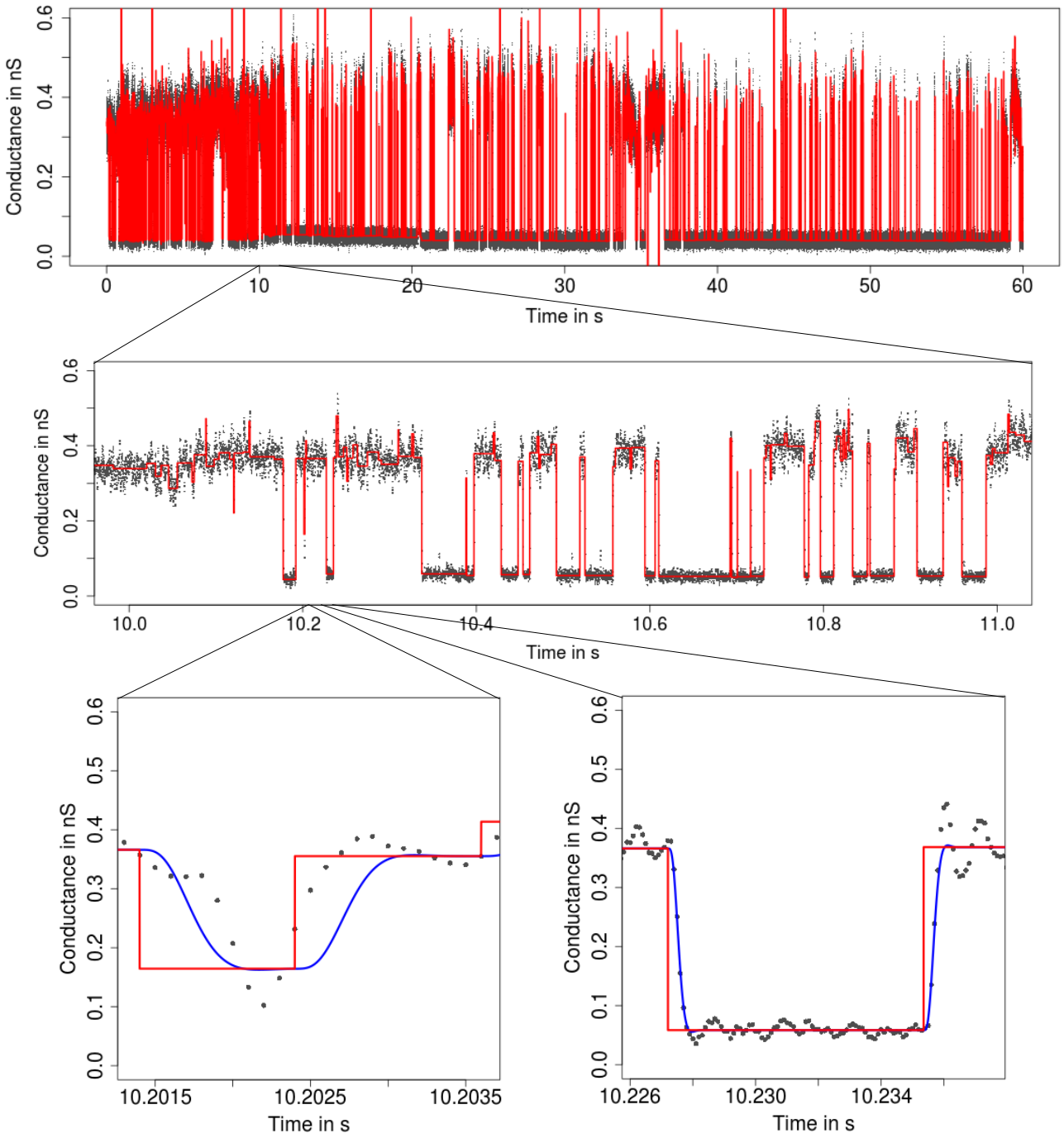

Fig. 3. Idealization (red) of the data in Figure 1 by JULES displayed on three different temporal scales. In the lower panels we also show the convolution of the idealization with the lowpass filter (blue). It detects short events, but finds many small events (which are most likely false positives) at parts of high conductance and high variance (see for instance the idealization of the observations around 0.36 nS in the middle panel). These detections hinder the decovolution (see for instance the lower left panel) and make the idealization unreliable.

conductance changes occur frequently which reduces the complexity to linear in the number of observations. For instance the 600 000 observations in Fig. 1 can be idealized in a few minutes on a standard laptop. A detailed discussion of the computational complexity is given in Section III-E.

F. Simulations

In Section IV we investigate the performance of HILDE in Monte-Carlo simulations which resemble the characteristics of the data in the application in Section V. Based on this we confirm that HILDE works very well for data sets like the one shown in Fig. 1. In more detail, it can detect events which last 0.2 ms, corresponding to only two subsequent observations and being less than one fifth of the filter length long, with probability almost one. Furthermore, all parameters (conductance levels and the locations of the changes) are estimated very accurately, see Section IV-B for more details. Moreover, two subsequent events can be separated reliably as soon as the distance between them is larger than five

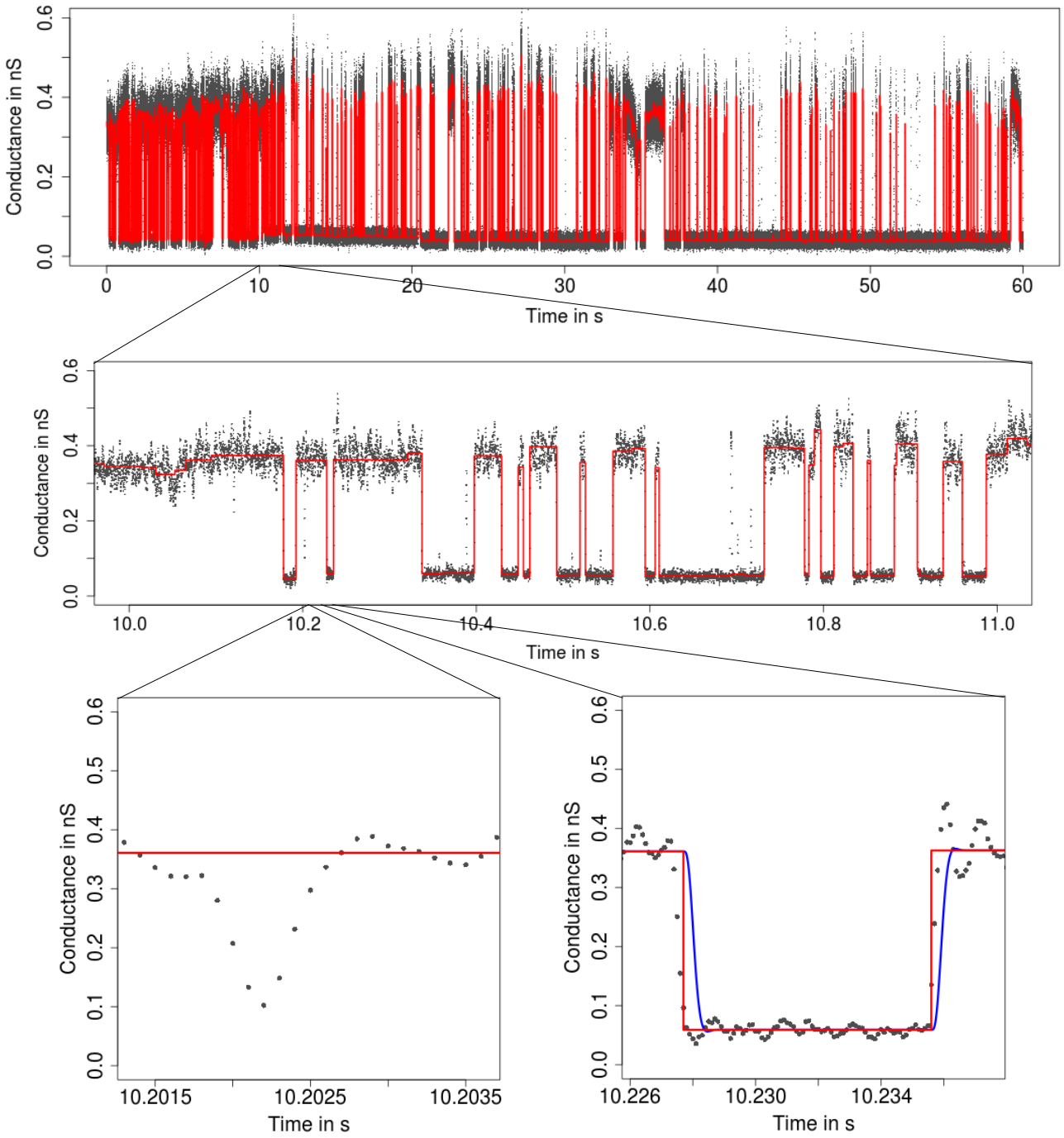

Fig. 4. Idealization (red) of the data in Figure 1 by HSMUCE displayed on three different temporal scales. In the lower panels we also show the convolution of the idealization with the lowpass filter (blue). It detects events on larger temporal scales well (middle panel, lower right panel), but misses short events, see for instance at around 10.2 s (lower left panel), 10.4 s or 10.7 s.

times the filter length, see Section IV-C. In Section IV-D we simulate data from a hidden Markov model. Our method is not assuming a HMM, but such a model is still illustrative to simulate as it is a standard assumption for the analysis of ion channel recordings. We will also see in Section V-C that a Markov model is reasonable for the PorB recordings. We find in Section IV-D that HILDE recovers all parameters with high precision. Those parameters are chosen similar to those which we have estimated in Section V-C. Finally, we investigate robustness issues against f^2- and $1/f$-noise in Section IV-E. We omit most of the time a systematic comparison with other approaches, since, as discussed in the introduction before, to the best of our knowledge all existing approaches assume a more restrictive model which hinders a fair comparison. However, we include JULES, HSMUCE and a HMM based approach in the simulations in Section IV-D to illustrate the shortcomings (and benefits) of these approaches further.

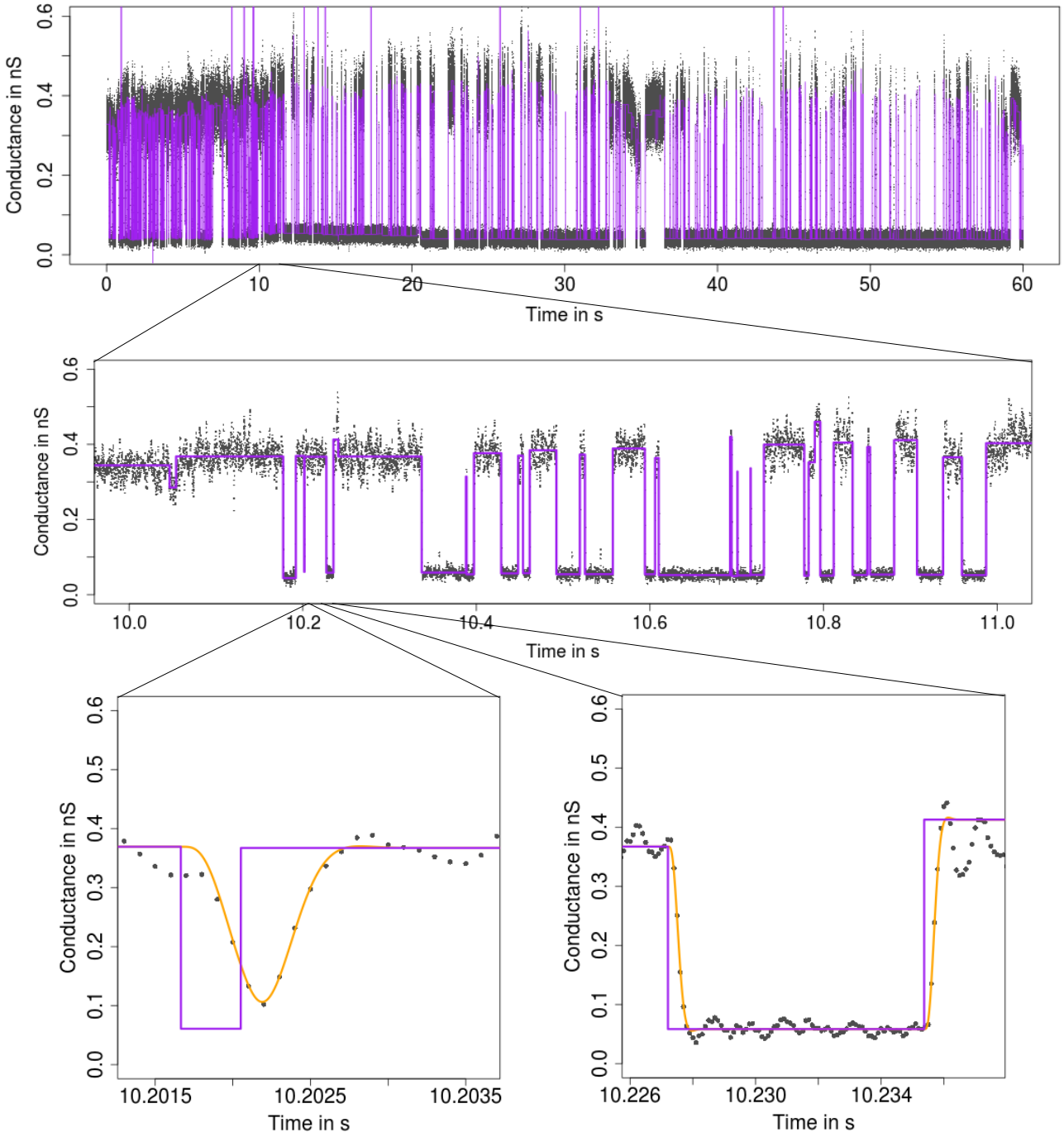

Fig. 5. Idealization (purple) of the data in Figure 1 by HILDE displayed on three different temporal scales. In lower panels we also show the convolution of the idealization with the lowpass filter (orange). HILDE idealizes events on all relevant temporal scales well.

G. Application to PorB Recordings

Our analysis of single channel recordings of PorB in Section V confirms all major results from [15] about this data set. Moreover, a novel finding of our analysis is that the dwell times do not fit a single exponential distribution, but suggests that two different regimes for the dwell times are underlying: very short openings of 2.31 ms estimated average duration and longer openings of 51.62 ms estimated average duration. To best of our knowledge, fast and slow gating at the same time was not observed for PorB before, but for another porine OmpG [34]. We stress that all results obtained by HILDE could be confirmed by at least one other approach. However, none of the other methods were able to reproduce all results obtained by HILDE.

In summary, in this work we propose with HILDE the first fully automatic model-free method for the analysis of ion channel recordings affected from open channel noise, i.e., to the best of our knowledge no other existing methodology is able to estimate a piecewise constant function in a model-free manner when filtering and heterogeneous noise are present at the same time. Simulations confirm that HILDE deals efficiently with heterogeneous noise and filtered data at the same

time and idealizes events on various time scales efficiently. More precisely, to obtain a good idealization events have to be only at least two subsequent observations long but separated from each other by at least five times the filter length (at signal and noise ratio and filtering as in the analyzed data). This allowed us to obtain novel findings for the PorB channel, e.g., that it can have shorter and longer opening processes at the same time.

II. Modeling

We assume that the recordings result from equidistant sampling from the convolution of an unknown piecewise constant signal corrupted by Gaussian white noise with the (known) kernel of a lowpass filter. We stress however that our methodology can be extended to an unknown filter by using the methodology of [37]. To incorporate heterogeneity, the white noise is scaled by an unknown piecewise constant function to allow a larger variance on segments on which the conductance is larger. We only allow potential variance changes when the conductance changes, since variance changes also depend on gating events of the channel. More precisely, we model the conductivity and the standard deviation by piecewise constant signals f and σ,

$$f(t) = \sum_{j=0}^{K} c_j \mathbb{1}_{[\tau_j, \tau_{j+1})}(t) \text{ and } \sigma(t) = \sum_{k=0}^{K} s_k \mathbb{1}_{[\tau_k, \tau_{k+1})}(t), \tag{II.1}$$

where t denotes physical time. The (unknown) conductance levels are denoted as $c_0, \dots, c_K$, the (unknown) standard deviations as $s_0, \dots, s_K > 0$, the (unknown) number of changes as K and the (unknown) locations as $-\infty =: \tau_0 < \tau_1 < \cdots < \tau_K < \tau_{K+1} := \tau_{\text{end}}$. The indicator function $\mathbb{1}_A(t)$ is one if $t \in A$ and zero otherwise. The signals are extended to $\tau_0 = -\infty$ to define the convolution correctly but we will see at the end of this section that only a very short time period before recordings started, i.e., before $t = 0$, will be relevant. We assume $c_k \neq c_{k+1}$ to define the number of changes unambiguously, i.e., to obtain an *identifiable* model. But we allow $s_k = s_{k+1}$, i.e., the standard deviation does not have to change between different events and in particular homogeneous noise is still part of the model ($\sigma \equiv s_0$). We stress that the class of signals in (II.1) is very flexible as potentially any arbitrary number of changes at arbitrary conductance levels and arbitrary standard deviations can be imposed, see Fig. 5 for an example.

We assume further that the recorded data points $Y_1, \dots, Y_n$ (the measured conductivity at time points $t_i = i/f_s$, $i = 1, \dots, n$, equidistantly sampled at rate f_s) result from convolving the signal f perturbed by Gaussian white noise η scaled by the standard deviation function σ with an analogue lowpass filter, with (truncated) kernel F_m, and digitization at sampling rate $f_s = n/\tau_{\text{end}}$, i.e.,

$$Y_i = \big(F_m * (f + \sigma\eta)\big)(i/f_s) = (F_m * f)(i/f_s) + \epsilon_i, \tag{II.2}$$

$i = 1, \dots, n$, with $*$ the convolution operator. Here, n denotes the total number of data points (typically several hundred thousands up to few millions). Like in [6], [7] we truncate (and rescale) the kernel of the lowpass filter and the covariance function at m/f_s to simplify our model. This is implemented in the `R` function *lowpassFilter* [36]. As a working rule, we choose m such that the autocorrelation function of the untruncated analogue lowpass filter is below 10^{-3} afterwards. For the later analyzed PorB traces, which are filtered by a 4-pole lowpass Bessel filter with 1 kHz cut-off frequency and sampled at 10 kHz, this choice leads to $m = 11$. Hence, in our model the resulting errors $\epsilon_1, \dots, \epsilon_n$ are Gaussian and centered, $\mathbb{E}[\epsilon_i] = 0$, and have covariance $\mathsf{Cov}[Y_i, Y_{i+j}]$

$$\sum_{k=0}^{K} s_k^2 \big[\mathcal{A}_m(i/f_s - \tau_k, j/f_s) - \mathcal{A}_m(i/f_s - \tau_{k+1}, j/f_s)\big] \tag{II.3}$$

for $j = -m, \dots, 0, \dots, m$, and 0 for $|j| > m$, with

$$\mathcal{A}_m(t, l) := \int_0^t F_m(s) F_m(s + l) ds. \tag{II.4}$$

Note that we have in (II.3) an unknown non-stationary covariance structure. However, the covariance can be decomposed into a known stationary autocorrelation given by the lowpass filter and an unknown non-stationary variance, which is modeled by a piecewise constant function σ that shares its change-points with the mean function and has to be estimated from the observations, see (B.5)–(B.9). An analytic expression of $\mathcal{A}_m(t, l)$ is implemented in the *R* function *lowpassFilter*. Hence, (II.3) can be computed exactly and efficiently.

The major aim will be now to idealize (reconstruct) the unknown signal f taking into account the convolution, the heterogeneous noise given by (II.3) and the specific structure of f in (II.1). This will be done fully automatically and with statistical error control. By fully automatic we mean that no user action is required during the idealization process, only certain errors levels $\alpha = \alpha_1 + \alpha_2$, the maximal scale on which local tests are performed $l_{\max}$ and two filter specific parameters have to be selected in advance, see Section III-A.

III. Methodology: HILDE

In this section we detail the three steps of our **H**eterogeneous **I**dealization by **L**ocal testing and **DE**convolution (HILDE) approach. A summary of these steps is given in the Meta-algorithm 1.

A. Parameter Choices

HILDE can be tuned by the parameters $\alpha_1, \alpha_2, l_{\max}$ and γ [2], see Algorithm 1 and the referenced sections for a definition. The probability to overestimate the number of conductance changes is approximately controlled by the sum of the error levels $\alpha = \alpha_1 + \alpha_2$. Hence, if such an overestimation control is desired, α should be chosen small. As a default choice we suggest $\alpha = 0.05$. Increasing α yields to a larger detection power (at the price of including more false positives). Hence, one may 'screen' for different α if important events are difficult to detect. The levels α_1 and α_2 allocates the power between the multiresolution test for detecting events on large scales ($> l_{\max}$) and the local tests to detect events on small scales ($\leq l_{\max}$), see Sections III-B and III-C, respectively.

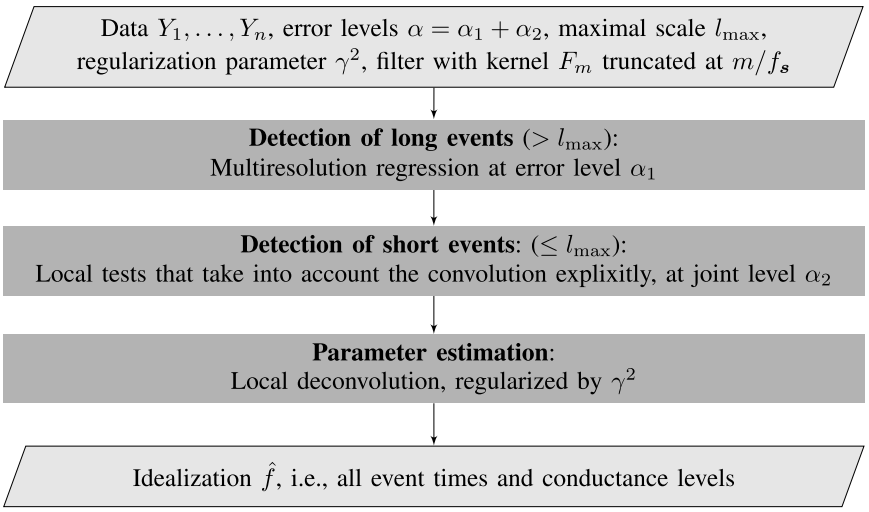

Algorithm 1. Steps of HILDE.

We have chosen $\alpha_2 = 0.04$ and $\alpha_1 = 0.01$ in our data analysis, since our focus was on detecting short events primarily, while events on larger scales were easier to detect. More weight can be put on α_1 if either short events are of less interest or if long events are difficult to detect as well, e.g. since they have a smaller jump size than the short events. The latter is often called *subgating* and was for instance studied in [6]. The tuning parameter $l_{\max}$, the largest scale on which local tests are performed to find short events, should be chosen such that all events on larger scales are detected by the previous multiresolution test. How long an event has to be to be detectable by the multiresolution test depends on the signal to noise ratio, on the used lowpass filter and on the tuning parameter α_1. An exact, but also computational demanding way to determine this length are Monte-Carlo simulations. Alternatively, the multiresolution step can be applied to a small data excerpt to explore which event lengths it is able to detect. Choosing $l_{\max}$ too small risks to miss events of length between $l_{\max}$ and the actual length that the multiresolution test requires, while a too large $l_{\max}$ only mildly decreases the detection power for all event lengths below $l_{\max}$. Hence, if one is in doubt, $l_{\max}$ should be chosen larger. In our setting, we choose $l_{\max} = 65$, since simulations (not displayed) showed that the multiresolution step in Section III-B is able to detect events which contain more than 65 observations with probability almost one. The correlation matrix is regularized with parameter $\gamma^2 = 1$, further details can be found in Section III B in [7]. And, as mentioned before, we truncate the kernel and autocorrelation function of the filter at $m = 11$ as the autocorrelation function is below 10^{-3} afterwards. All of these choices are the default parameters of the function *hilde* and are used in the simulations in Section IV and in the real data application in Section V.

B. Detection of Long Events

To detect events on larger temporal scales, we use a modification of the **H**eterogeneous **S**imulataneous **MU**ltiscale **C**hange-point **E**stimator, HSMUCE from [33], which is a multiresolution procedure that is robust against heterogeneous noise. To avoid false positives due to the filter, we omit on each interval the first m observations and do not test on very short intervals. Since we truncated the filter, the signal and the convolution of the signal with the lowpass filter differ only at the beginning of each segment. More precisely, if the signal is constant on an interval $[i/f_s, j/f_s]$ with conductance level c_{ij} and the first m observations $Y_i, \ldots, Y_{i+m-1}$ are ignored, all other observations $Y_{i+m}, \ldots, Y_j$ have constant expectation equal to the conductance level c_{ij}. Hence, we take into account only intervals longer than m/f_s and ignore the first m observations of each interval.

This leads to an estimator that detects change-points at presence of heterogeneous noise and filtering, i.e., when the heterogeneous ion channel model from Section II is assumed, while at the same time the probability to overestimate the number of events is controlled, i.e., a false positive is only added with probability at most equal to the tuning parameter α_1, see Theorem A.1 in Appendix A in the supplement. A detailed definition of this estimator is given in Appendix A in the supplement. Note that it does not take into account the convolution explicitly but still has good detection properties if events are long enough, but almost no detection power on small scales. Simulations (not displayed) show that for our data set events with of length at least 6.5 ms, corresponding to 65 sampling points, are detected reliably.

In the following two sections we will present a refinement of this idealization to detect and idealize events on smaller time scales, too, which proves to be relevant for our data example. Note that in this section and in the next section (a refinement will be provided in the local deconvolution step) we restrict all changes to the grid on which the observations are given, in other words, we assume that $f_s \tau_i$ are integers.

C. Detection of Short Events

To detect short events, we test on all intervals containing $l = 1, \ldots, l_{\max}$ (to be defined later) observations whether the previous idealization is the underlying signal or whether the

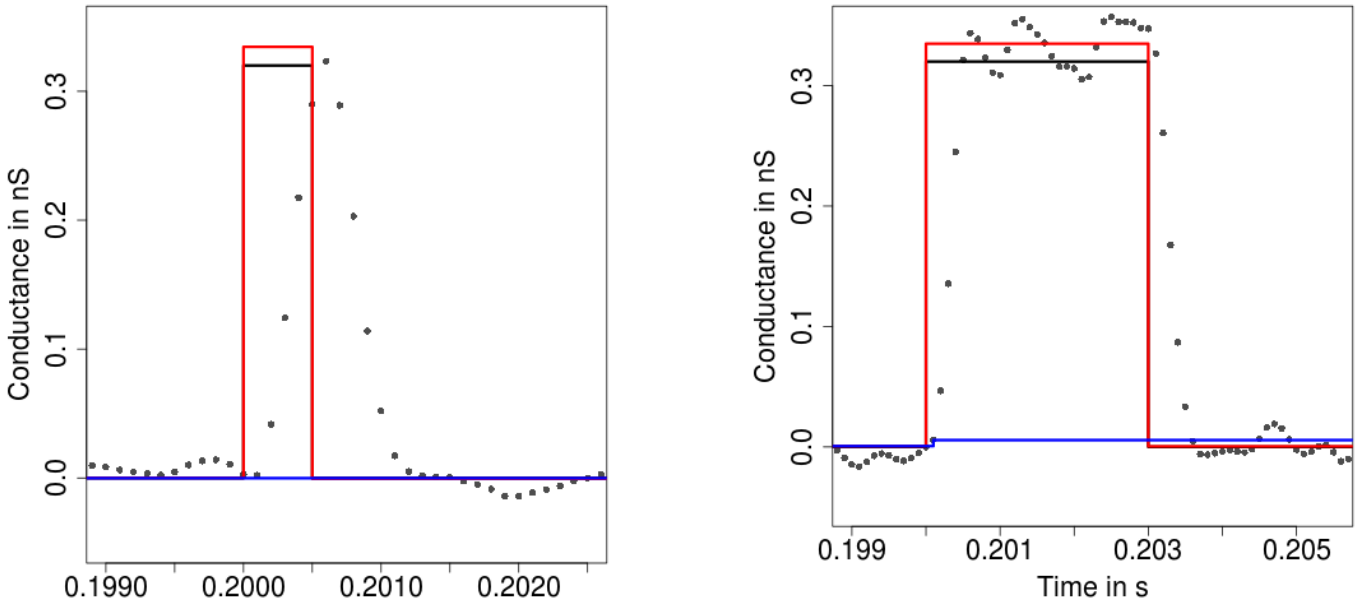

(a) The multiresolution step detects no events.

(b) The multiresolution step detects a (small) single change.

Fig. 6. Illustration of the testing process for short events. Simulated observations (grey points) with an underlying true signal f (black lines) that contains a short event. The hypothesis $f_0(t)$, obtained from the fit in the multiresolution step (blue lines), is tested against the alternative $f_1(c)(t)$ (red lines), which contains an additional short event. For details how to obtain the hypothesis and alternative see the paragraph '*Obtaining the hypotheses and alternatives*' in Appendix B in the supplement. If the test rejects, the short event is added to the fit and the final idealization will be obtained by deconvolution, see Fig. 7.

inclusion of an additional event on the considered interval is significantly better. If a test rejects, we add a short peak to the previous idealization. This peak potentially replaces a single change, in the following denoted by τ. This process is illustrated in Fig. 6.

More precisely, let $[\tau_L, \tau_R] = [i/f_s, j/f_s]$ be the interval on which we test. And assume for the moment that τ is the only change in $[(i-m+1)/f_s, (j+m-1)/f_s]$ with conductance levels c_L before and c_R afterwards. Note that this also includes the scenario of no change in $[(i-m+1)/f_s, (j+m-1)/f_s]$ by setting $c_L = c_R$. Then, we decide whether an additional event on $[\tau_L, \tau_R]$ is required by testing the hypothesis

$$f_0(t) = \begin{cases} c_L, & \text{if } t < \tau, \\ c_R, & \text{if } t \geq \tau \end{cases} \tag{III.1}$$

against the alternative

$$f_1(c)(t) = \begin{cases} c_L, & \text{if } t < \tau_L, \\ c, & \text{if } \tau_L \leq t < \tau_R, \\ c_R, & \text{if } t \geq \tau_R, \end{cases} \tag{III.2}$$

with $c \in \mathbb{R}$ arbitrary. The form of the hypothesis and alternative is illustrated in Fig. 6. The same structure is assumed for standard deviation functions σ_0 and σ_1 with values s_L, s and s_R. The precise hypotheses and alternatives, i.e., the values for τ, c_L, c_R, s_L and s_R, are determined by the previous idealization step. If more than one change is contained in $[(i-m+1)/f_s, (j+m-1)/f_s]$, no local test will be performed on this interval. The reasoning behind this and how to obtain τ, c_L, c_R, s_L and s_R exactly are explained in the paragraph '*Obtaining the hypotheses and alternatives*' in Appendix B in the supplement. All tests are performed at simultaneous error level $\alpha_2 > 0$.

The form of these hypotheses allows us to construct a test statistic that takes into account the convolution explicitly. Moreover, information provided by potential variance changes can be used as well. We provide details of the corresponding test in the paragraph '*Local testing*' in Appendix B in the supplement. All choices there are motivated by a trade-off between a good detection power for events in the measurements in Section V, see Fig. 1, and a reasonable computational complexity.

If a hypothesis is rejected, we replace the single change-point at τ by a short peak, i.e., the initial fit $f_0(\cdot)$ is replaced by $f_1(c)(\cdot)$. Temporary locations will be placed at $\tau_L = i/f_s$ and $\tau_R = j/sr$, but exact locations and the conductance level c will be obtained in the upcoming deconvolution step. However, note that usually one event in the data causes rejections of multiple tests. Therefore, we only consider the event with the largest test statistic among all rejections on intervals that intersect or adjoin each other. More details are provided in the paragraph '*Multiple dependent rejections*' in Appendix B in the supplement.

D. Parameter Estimation by Local Deconvolution

The final idealization is obtained by local deconvolution as described in Section 3.2 of [7] with two adjustments, which will be discussed in Appendix C in the supplement. This means in particular that we still use the likelihood function of observations with homogeneous noise, although heterogeneous noise is assumed. Simulations show, see Section IV, that

this works reasonably well for the recordings we analyze in Section V. Alternatives for recordings with more pronounced noise heterogeneity are discussed in Section VI-A.

E. Computation and Run Time

The multiresolution regression step in Section III-B can be computed by a pruned dynamic program as described in Section A.1 in the supplement of [33]. For related ideas, see also [32], [38]–[40] and the references given there. The implementation of the local tests in Section III-C is straightforward. The local deconvolution in Section III-D can be computed by an iterative grid search as described in Section 3.2 of [7]. An implementation of HILDE is available by the `R` function *hilde* in the package *clampSeg*. The package is available on request and has been submitted parallel to CRAN [36]. All run time critical parts are written in C++ and are interfaced by the `R` code.

The worse case computation complexity of the dynamic program is quadratic in the number of observations n. However, in most ion channel recordings conductance changes occur frequently which reduces the complexity to be linear $\mathcal{O}(n)$, see Section A.3 in the supplement of [33]. The local tests in Section III-C are of complexity $\mathcal{O}(l_{\max}^2\, n)$, since for each of the $l_{\max}$ scales $1, \dots, l_{\max}$ roughly n tests have to be performed and the complexity to compute a single test is at most of order $\mathcal{O}(l_{\max})$. The computation time of the local deconvolution is dominated by the iterative grid search to deconvolve a single event. The deconvolution of a single event is constant in the number of observations, since the number of involved observations and the grid sizes do not increase. Moreover, the number of involved observations is small and the covariance matrix is a band matrix, with band size equal to m, which allows fast computation. Hence, the complexity of the deconvolution increases linearly in the number of events which increases for ion channel recordings typically linearly in the number of observations. In summary, for a typical channel trace the complexity to compute HILDE increases only linearly in the number of observations. This is confirmed by a run time of less than five minutes for idealizing the 600 000 observations in Fig. 1 on a Dell Latitude E6530 with Intel(R) Core(TM) i5-3340M CPU 2.70GHz processor. Similar run times are obtained for the traces generated in Section IV-D. Thus, the theoretical considerations as well as the empirical run times confirm that HILDE can be computed efficiently, which is important since large data sets have to be analyzed.

IV. Simulations

In this section we examine the performance of HILDE in Monte-Carlo simulations. Since to our best knowledge no other model-free method is known that takes into account heterogeneous noise and filtering explicitly, it is difficult to compare HILDE with other methods. Most similar in spirit are JULES [7], HSMUCE and an HMM based approach [41]. These have been included in a simulation in Section IV-D for purpose of comparison. The simulation study consists of four parts. First of all, we investigate the detection and idealization of isolated peaks. Secondly, we identify the minimal distance at which HILDE is able to separate two consecutive peaks. Thirdly, although HILDE does not rely on a hidden Markov model assumption, we examine its ability to recover the parameters of a Markov model, since a hidden Markov model is a common assumption for ion channel recordings. Finally, we investigate its robustness against violations of the model in Section II, in particular against additional f^2 and $1/f$ noise.

A. Data Generation

We generate all signals and observations accordingly to the heterogeneous ion channel model we described in Section II and such that they are in line with the measured data we analyze in Section V. This means in particular that amplitudes, dwell times and noise levels of the generated observations are chosen such that they are similar to those of the analyzed datasets. We also simulate a 4-pole Bessel filter with 1 kHz cut-off frequency and sample the observation at 10 kHz.

The expectation of the observations, given by the convolution of the signal with the truncated kernel F_m of the lowpass Bessel filter, can be computed explicitly. For the errors we oversample by a factor of 100, i.e., we generate 100 times as many independent Gaussian observations, discretize the filter accordingly, compute a discrete convolution and rescale the observations such that they have the desired standard deviation.

B. Isolated Peak

In this simulation with 4 000 observations we examine the detection and idealization of a single isolated peak. More precisely, in accordance with the model in Section II and with the estimated values in Section V for the observations in Fig. 1, we choose conductance levels $c_0 = c_2 = 0$, $c_1 = 0.32$, variances $s_0^2 = s_2^2 = 6.1 \cdot 10^{-5}$ and varying variance $s_1^2 \in \{2 \cdot 10^{-4}, 5 \cdot 10^{-4}, 10^{-3}, 2 \cdot 10^{-3}, 5 \cdot 10^{-3}\}$ to examine the influence of different noise levels. Note that $s_1^2 = 10^{-3}$ is roughly the noise level in the measurements in Section V. Moreover, we simulate changes at $\tau_1 = 2000/f_s$ and $\tau_2 = (2000 + \ell)/f_s$, c.f. (II.1), and are interested in how well HILDE detects the peak and idealizes the locations τ_1 and τ_2 and the level l_1 as a function of ℓ, the length (relative to the sampling rate f_s) of the peak. For $\ell = 5$, Fig. 7 shows an example of the simulated data as well as the idealizations by HILDE and their convolutions with the Bessel filter in a neighborhood of the peak. Tables II–IV summarize our results based on 10 000 repetitions for $\ell = 2, 3, 5$.

To this end, we count how often the signal is *correctly identified*, i.e., only the peak and no other change is detected. More precisely, we define the peak as *detected* if there exists a j such that $|\hat{\tau}_j - \tau_1| < m/f_s$ and $|\hat{\tau}_{j+1} - \tau_2| < m/f_s$ as a peak is shifted at most m/f_s by the filter. If only one change but not a peak is within these boundaries we do not count it as a true detection, but also not as a *false positive*, whereas all other changes are counted as *false positives*. For the estimated locations and the level we only consider cases where the peak is detected and report the mean square error, the bias and the standard deviation.

TABLE II

PERFORMANCE OF HILDE IN IDEALIZING A SIGNAL WITH AN ISOLATED PEAK IN DIFFERENT SETTINGS. THEY DIFFER IN THE AMOUNT OF OPEN CHANNEL NOISE AND THE LENGTH OF THE PEAK. MORE PRECISELY, IT HAS CHANGES AT $\tau_1 = 0.2$ AND $\tau_2 = \tau_1 + \ell/f_s$, $\ell = 2,3,5$, CONDUCTANCE LEVELS $c_0 = c_2 = 0$, $c_1 = 0.32$, VARIANCES $s_0^2 = s_2^2 = 6.1 \cdot 10^{-5}$ AND VARYING VARIANCE $s_1^2 \in \{2 \cdot 10^{-4}, 5 \cdot 10^{-4}, 10^{-3}, 2 \cdot 10^{-3}, 5 \cdot 10^{-3}\}$. RESULTS ARE BASED ON 10 000 PSEUDO SAMPLES. AN EXAMPLE, $s_1^2 = 10^{-3}$ AND $\ell = 5$, IS GIVEN IN FIGURE 7

Setting	Length (ℓ)	Correctly identified (%)	Detected (%)	False positive (Mean)
$s_1^2 = 2 \cdot 10^{-4}$	2	99.96	100.00	0.0008
$s_1^2 = 5 \cdot 10^{-4}$	2	99.96	100.00	0.0008
$s_1^2 = 10^{-3}$	2	99.94	99.98	0.0010
$s_1^2 = 2 \cdot 10^{-3}$	2	99.07	99.11	0.0014
$s_1^2 = 5 \cdot 10^{-3}$	2	90.04	90.08	0.0042
$s_1^2 = 2 \cdot 10^{-4}$	3	99.97	100.00	0.0006
$s_1^2 = 5 \cdot 10^{-4}$	3	99.97	100.00	0.0006
$s_1^2 = 10^{-3}$	3	99.97	100.00	0.0006
$s_1^2 = 2 \cdot 10^{-3}$	3	99.93	99.96	0.0006
$s_1^2 = 5 \cdot 10^{-3}$	3	96.08	96.11	0.0024
$s_1^2 = 2 \cdot 10^{-4}$	5	99.95	100.00	0.0010
$s_1^2 = 5 \cdot 10^{-4}$	5	99.95	100.00	0.0010
$s_1^2 = 10^{-3}$	5	99.95	100.00	0.0010
$s_1^2 = 2 \cdot 10^{-3}$	5	99.94	100.00	0.0012
$s_1^2 = 5 \cdot 10^{-3}$	5	99.42	99.48	0.0018

TABLE III

PERFORMANCE OF HILDE IN IDEALIZING A SIGNAL WITH AN ISOLATED PEAK IN DIFFERENT SETTINGS. THEY DIFFER IN THE AMOUNT OF OPEN CHANNEL NOISE AND THE LENGTH OF THE PEAK. MORE PRECISELY, IT HAS CHANGES AT $\tau_1 = 0.2$ AND $\tau_2 = \tau_1 + \ell/f_s$, $\ell = 2,3,5$, CONDUCTANCE LEVELS $c_0 = c_2 = 0$, $c_1 = 0.32$, VARIANCES $s_0^2 = s_2^2 = 6.1 \cdot 10^{-5}$ AND VARYING VARIANCE $s_1^2 \in \{2 \cdot 10^{-4}, 5 \cdot 10^{-4}, 10^{-3}, 2 \cdot 10^{-3}, 5 \cdot 10^{-3}\}$. RESULTS ARE BASED ON 10 000 PSEUDO SAMPLES AND ARE GIVEN AS MULTIPLES OF THE SAMPLING RATE $f_s = 10^4$. AN EXAMPLE, $s_1^2 = 10^{-3}$ AND $\ell = 5$, IS GIVEN IN FIGURE 7

Setting	Length (ℓ)	f_s^2MSE($\hat{\tau}_1$)	f_sBIAS($\hat{\tau}_1$)	f_sSD($\hat{\tau}_1$)	f_s^2MSE($\hat{\tau}_2$)	f_sBIAS($\hat{\tau}_2$)	f_sSD($\hat{\tau}_2$)
$s_1^2 = 2 \cdot 10^{-4}$	2	0.0331	0.0092	0.1818	0.0381	-0.0076	0.1951
$s_1^2 = 5 \cdot 10^{-4}$	2	0.0515	0.0113	0.2267	0.0427	-0.0115	0.2062
$s_1^2 = 10^{-3}$	2	0.0677	0.0255	0.2590	0.0595	-0.0266	0.2424
$s_1^2 = 2 \cdot 10^{-3}$	2	0.1532	0.0935	0.3801	0.1570	-0.0942	0.3848
$s_1^2 = 5 \cdot 10^{-3}$	2	0.6628	0.3275	0.7454	0.6223	-0.3252	0.7188
$s_1^2 = 2 \cdot 10^{-4}$	3	0.0120	0.0001	0.1097	0.0117	0.0010	0.1083
$s_1^2 = 5 \cdot 10^{-4}$	3	0.0177	0.0040	0.1329	0.0177	-0.0022	0.1332
$s_1^2 = 10^{-3}$	3	0.0391	0.0181	0.1970	0.0388	-0.0152	0.1965
$s_1^2 = 2 \cdot 10^{-3}$	3	0.1569	0.0846	0.3870	0.1533	-0.0802	0.3833
$s_1^2 = 5 \cdot 10^{-3}$	3	1.1681	0.4668	0.9748	1.1058	-0.4515	0.9498
$s_1^2 = 2 \cdot 10^{-4}$	5	0.0070	-0.0014	0.0835	0.0084	0.0013	0.0914
$s_1^2 = 5 \cdot 10^{-4}$	5	0.0176	0.0036	0.1326	0.0189	-0.0037	0.1375
$s_1^2 = 10^{-3}$	5	0.0572	0.0217	0.2381	0.0591	-0.0215	0.2421
$s_1^2 = 2 \cdot 10^{-3}$	5	0.2473	0.0985	0.4874	0.2464	-0.0976	0.4867
$s_1^2 = 5 \cdot 10^{-3}$	5	2.0808	0.6363	1.2946	2.1605	-0.6520	1.3174

TABLE IV

PERFORMANCE OF HILDE IN IDEALIZING A SIGNAL WITH AN ISOLATED PEAK IN DIFFERENT SETTINGS. THEY DIFFER IN THE AMOUNT OF OPEN CHANNEL NOISE AND THE LENGTH OF THE PEAK. MORE PRECISELY, IT HAS CHANGES AT $\tau_1 = 0.2$ AND $\tau_2 = \tau_1 + \ell/f_s$, $\ell = 2,3,5$, CONDUCTANCE LEVELS $c_0 = c_2 = 0$, $c_1 = 0.32$, VARIANCES $s_0^2 = s_2^2 = 6.1 \cdot 10^{-5}$ AND VARYING VARIANCE $s_1^2 \in \{2 \cdot 10^{-4}, 5 \cdot 10^{-4}, 10^{-3}, 2 \cdot 10^{-3}, 5 \cdot 10^{-3}\}$. RESULTS ARE BASED ON 10 000 PSEUDO SAMPLES. AN EXAMPLE, $s_1^2 = 10^{-3}$ AND $\ell = 5$, IS GIVEN IN FIGURE 7

Setting	Length (ℓ)	MSE($\hat{c}_1$)	BIAS($\hat{c}_1$)	SD($\hat{c}_1$)
$s_1^2 = 2 \cdot 10^{-4}$	2	0.1320	0.0194	0.3628
$s_1^2 = 5 \cdot 10^{-4}$	2	0.6953	0.0322	0.8333
$s_1^2 = 10^{-3}$	2	2.3290	0.0888	1.5236
$s_1^2 = 2 \cdot 10^{-3}$	2	21.7896	0.7801	4.6025
$s_1^2 = 5 \cdot 10^{-3}$	2	294.6030	5.5640	16.2380
$s_1^2 = 2 \cdot 10^{-4}$	3	0.0002	0.0009	0.0152
$s_1^2 = 5 \cdot 10^{-4}$	3	0.0007	0.0018	0.0259
$s_1^2 = 10^{-3}$	3	0.0023	0.0055	0.0473
$s_1^2 = 2 \cdot 10^{-3}$	3	1.7338	0.0806	1.3143
$s_1^2 = 5 \cdot 10^{-3}$	3	334.7102	5.0891	17.5739
$s_1^2 = 2 \cdot 10^{-4}$	5	0.0001	0.0001	0.0077
$s_1^2 = 5 \cdot 10^{-4}$	5	0.0003	0.0007	0.0179
$s_1^2 = 10^{-3}$	5	0.0013	0.0033	0.0354
$s_1^2 = 2 \cdot 10^{-3}$	5	0.0055	0.0158	0.0725
$s_1^2 = 5 \cdot 10^{-3}$	5	203.0129	2.7499	13.9811

In most scenarios, HILDE has a good detection power and detects almost no false positives, see Table II. Only for a five times larger variance than in the real data and when $l \leq 3$ few events are missed. In Tables III and IV we found that idealization of the locations τ_1 and τ_2 and the conductance value c_1 works well for variances similar to the real data, but has some issues when the variance of the peak is larger, in particular in the scenario of a five times larger variance. For such observations it might be desirable to take into account the heterogeneous noise in the deconvolution step,

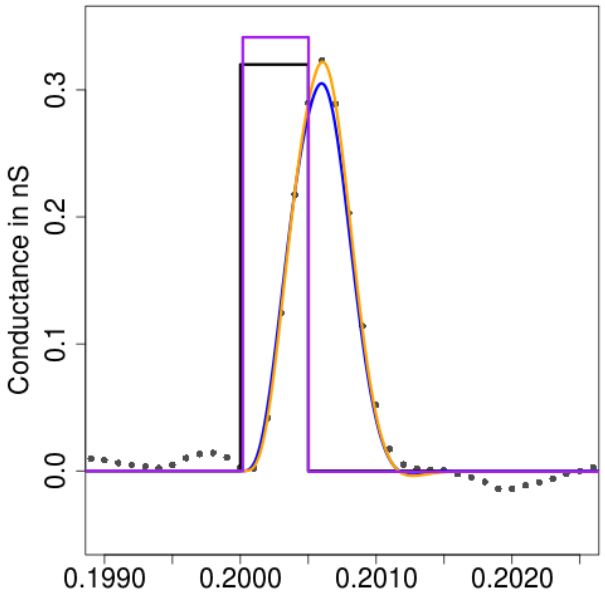

Fig. 7. Simulated observations (grey points), true block signal f (black line) and its convolution (blue line), HILDEs idealization (purple line) and its convolution (orange line) with the lowpass 4-pole Bessel filter. HILDE provides very accurate idealization.

see Section VI-A for more details. For smaller variances the results for estimating the locations are better when the peak is longer, but for larger variances results are even worse when the peak is longer. An explanation might be two effects with opposite influences. The conductance change provide more information when the peak is longer, but then also the overall variance of the observations is larger which reduces estimation accuracy. Estimation of the level c_1 is always more accurate when the peak is longer. It seems that here the first effect dominates.

All in all, these simulations confirm that HILDE performs very well for observations comparable to them in Section V.

C. Separation of Two Consecutive Peaks

To examine how well HILDE separates two consecutive peaks we perform the same simulations as in Section 4.3 in [7], since results are identical for homogeneous and heterogeneous noise as separation depends on the method and distance between the peaks but not on the noise level. More precisely, we consider a signal f with changes at $\tau_1 = 2\,000/f_s$, $\tau_2 = \tau_1 + 5/f_s$, $\tau_3 = \tau_2 + d$ and $\tau_4 = \tau_3 + 5/f_s$,, with $\tau_0 = 0$ and $\tau_{\text{end}} = 4\,000/f_s$ and levels $l_0 = l_2 = l_4 = 40\,\text{pS}$ and $l_1 = l_3 = 20\,\text{pS}$. Hence d is the distance between the two peaks. We distinguish between perfect separation, i.e., the detection step of HILDE identifies the two peaks (4 changes) and the local deconvolution yields idealizations for the four levels (illustrated in Fig. 8c). Secondly, separation fails in the detection step, i.e., the multiresolution reconstruction recognizes only 2 changes and identifies one peak whose level can be further deconvolved (illustrated in Fig. 8a). Finally, idealizing two peaks fails in the deconvolution step, i.e., HILDE identifies two peaks but the distance is so small that a local deconvolution cannot be applied, in other words, no long segment is in between (illustrated in Fig. 8b).

Fig. 9 shows the frequency at which each scenario occurred as a function of d, the distance between the two peaks, in 10 000 simulations for each value of $d = \{1, 2, \ldots, 70\}$. We found that the two peaks are detected if $d > 6$, but local deconvolution and hence an appropriate idealization requires $d \geq 62$. Hence, in Section V events have to be separated by more than 6.2 ms to be idealized appropriately. In comparison, we found that events are on average separated by $1/(2.67 + 4.50)\,\text{s} \approx 0.14\,\text{s}$ which shows that this limitation is not an issue for the analyzed PorB recordings.

D. Hidden Markov Model

In this section we simulate data from a three state hidden Markov model. Since hidden Markov models are often assumed for ion channel recordings, it is instructive to investigate the methods in such a scenario. We simulate observations that resemble the PorB data we analyze in Section V. More precisely, we have expectations 0 nS, 0 nS and 0.32 nS as well as standard deviations 0.0078 nS, 0.0078 nS and 0.0316 nS, i.e. the variances are $6.1 \cdot 10^{-5}(\text{nS})^2$ and $10^{-3}(\text{nS})^2$. The dwell times in the first, second and third state are exponentially distributed with rates 20 Hz, 400 Hz and 7 Hz, respectively. The process always jumps from the first or second state to the third state, i.e., no transitions between the first and second state are allowed. And it jumps from the third state with probability $2/3$ to the first state and with probability $1/3$ to the second state. We generate five time series with 600 000 observations, each. Each trace looks similar to the observations in Fig. 1 and hence we refrain from showing an example.

We analyze these data sets with HILDE and for purpose of comparison with JULES [7], HSMUCE [33] and an HMM based approach which assumes the true three state model, i.e. three states, whereby two have the same expectations and variances and no transitions are allowed between them. We used

$$\mu = (0, 0, 0.32)^T,$$
$$s = (0.0102, 0.0102, 0.0321)^T,$$
$$P = \begin{pmatrix} 0.999 & 0 & 0.001 \\ 0 & 0.99 & 0.01 \\ 0.02 & 0.03 & 0.95 \end{pmatrix}.$$

as starting values for the Baum-Welch algorithm. Those standard deviations were determined by taking the empirical standard deviation of all observations below and above 0.2, respectively. Idealizations are obtained by using a Viterbi algorithm.

The Baum-Welch algorithm estimated the following parameters

$$\mu = (0, 0, 0.3177)^T,$$
$$s = (0.0079, 0.0079, 0.0374)^T,$$
$$P = \begin{pmatrix} 0.999356 & 0 & 0.000644 \\ 0 & 0.997329 & 0.002671 \\ 0.002617 & 0.000089 & 0.997294 \end{pmatrix}.$$

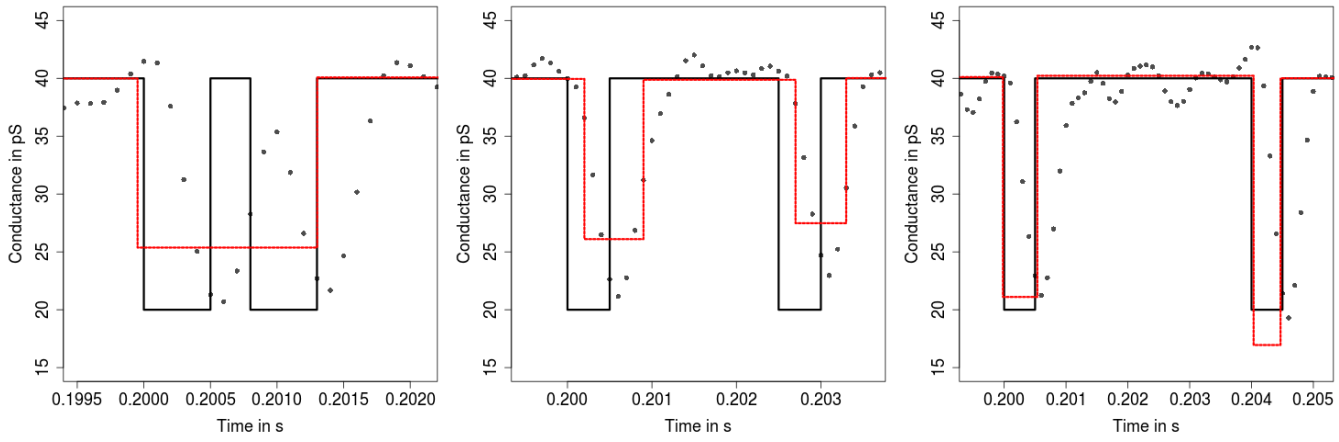

(a) No separation in the detection step, $d = 3$ (b) No local deconvolution can be applied, $d = 20$ (c) Perfect separation, $d = 35$

Fig. 8. Data $y_i = F * (f(i/n) + \sigma_0 \epsilon_i)$ (grey points), where $\sigma_0 = 1.4$, ϵ_i is gaussian white noise and the signal f has two consecutive peaks comprised of the levels $l_0 = l_2 = l_4 = 40$, $l_1 = l_3 = 20$ and change-points $\tau_1 = 2000/f_s$, $\tau_2 = \tau_1 + 5/f_s$, $\tau_3 = \tau_2 + d$ and $\tau_4 = \tau_3 + 5/f_s$. True signal (——) and JULES idealization (.....).

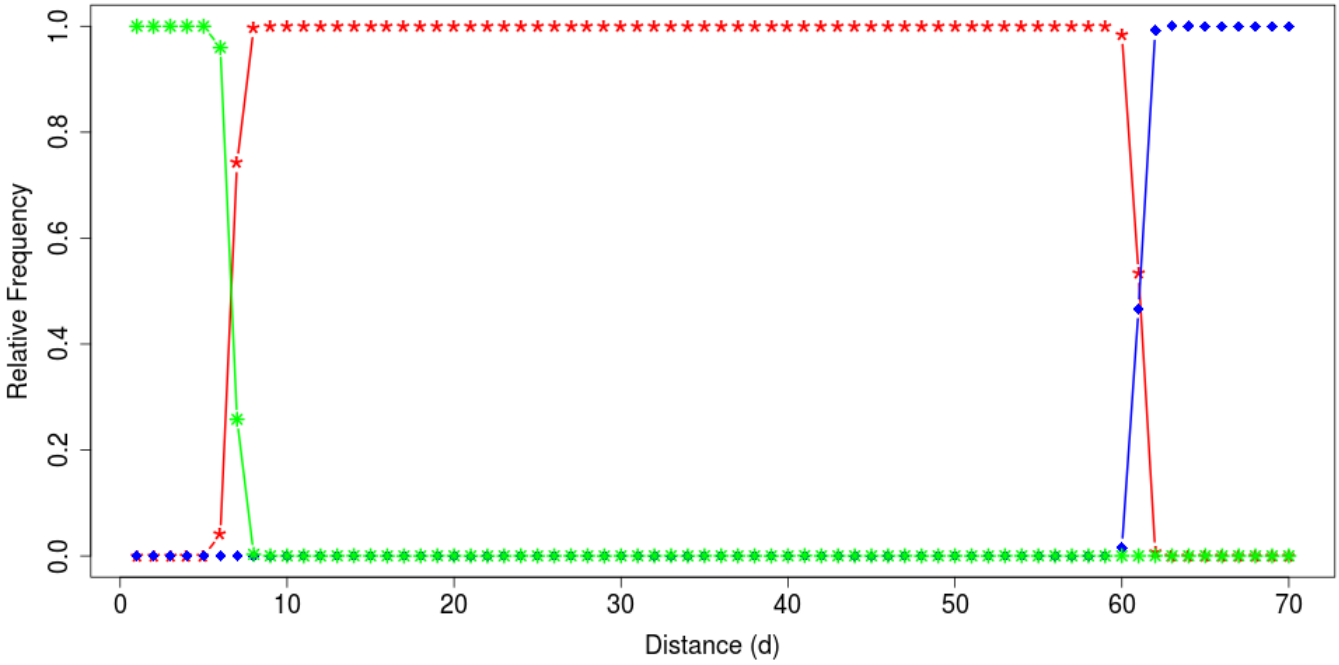

Fig. 9. Results for HILDE assuming heterogeneous noise in idealizing two consecutive peaks separated by distance d. Its frequencies for no separation in the detection step (∗), for successful detection, but no local deconvolution (⋆) and for successful detection and deconvolution (⧫). Results are based on 10 000 simulations for each value of d.

We will discuss the estimated transition matrix later in comparison with the other approaches and when we also discuss the results using the Viterbi algorithm. The estimated expectations and standard deviations are accurate. For the other approaches we show in Fig. 10 histograms of the estimated amplitudes of all events with an amplitude between 0.2 nS and 0.5 nS.

We found in Fig. 10 that all approaches estimate the amplitude accurately. The estimated amplitudes of HSMUCE are skewed, but the final estimation is still decent.

We continue with an analysis of the dwell times. To this end, we consider from now on all events with estimated conductance level between −0.05 nS and 0.05 nS as a closed event and between 0.15 nS and 2 nS as an open event, while all other events are considered as artifacts and are ignored. Fig. 11 shows histograms of the dwell times in the closed state for various approaches.

We see that with the exception of HSMUCE (it misses short events) none on the histograms look exponentially distributed, since we have a mixture of short and long events. Hence, in Figs. 12 and 13 we will analyze short and long events separately. To this end, we say an event is short if its dwell time is between 0.1 ms and 5 ms and long if its dwell time is between 20 ms and 200 ms. To estimate the rates, we apply a missed event correction like in [7].

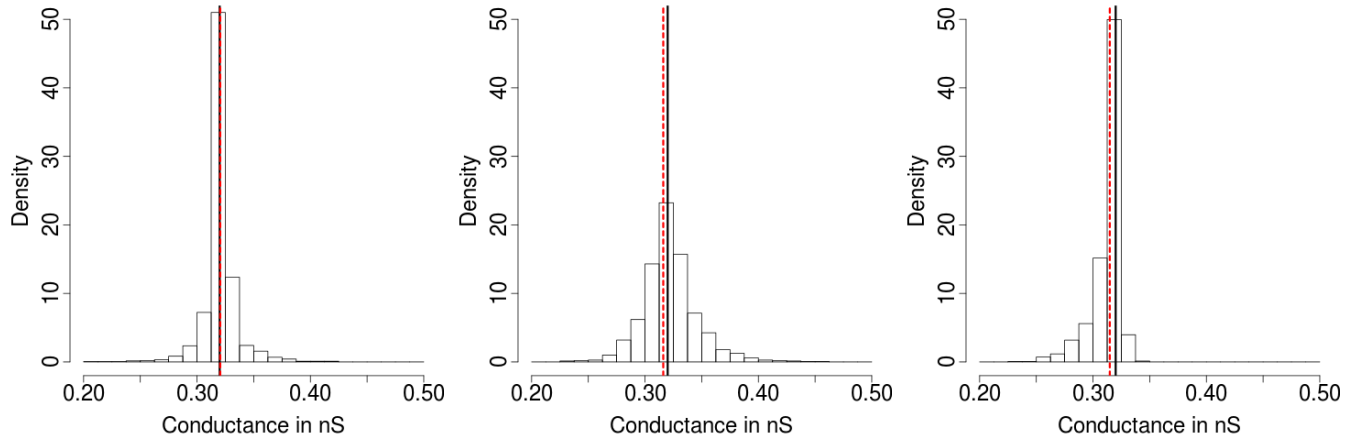

(a) HILDE (b) JULES (c) HSMUCE

Fig. 10. Histograms of the estimated amplitudes using various idealization approaches. (—) indicates the true amplitude of 0.32 and (.....) the estimated amplitudes of 0.3205, 0.3161 and 0.3148 by the half sample mode using the idealizations from HILDE, JULES and HSMUCE, respectively.

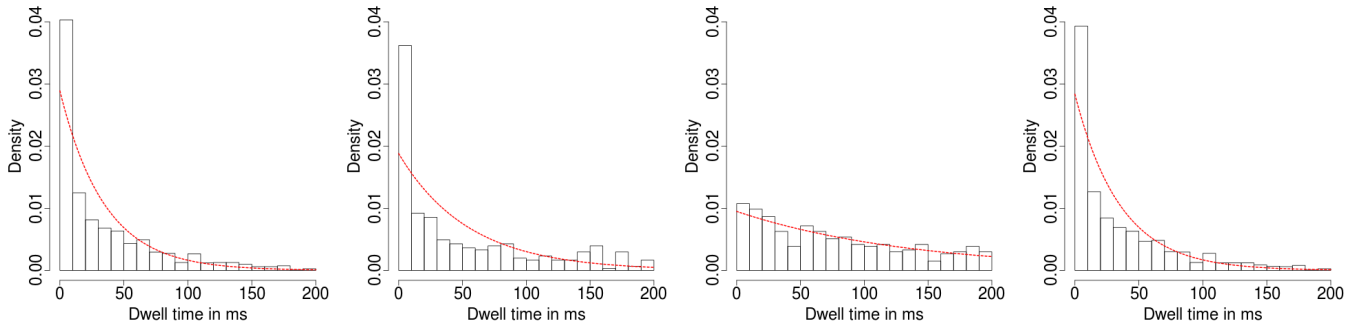

(a) HILDE (b) JULES (c) HSMUCE (d) HMM

Fig. 11. Histograms of the dwell times in the closed state with exponential fits (.....). We rescaled all lines such that the area under them are standardized to one to make them comparable to the histograms.

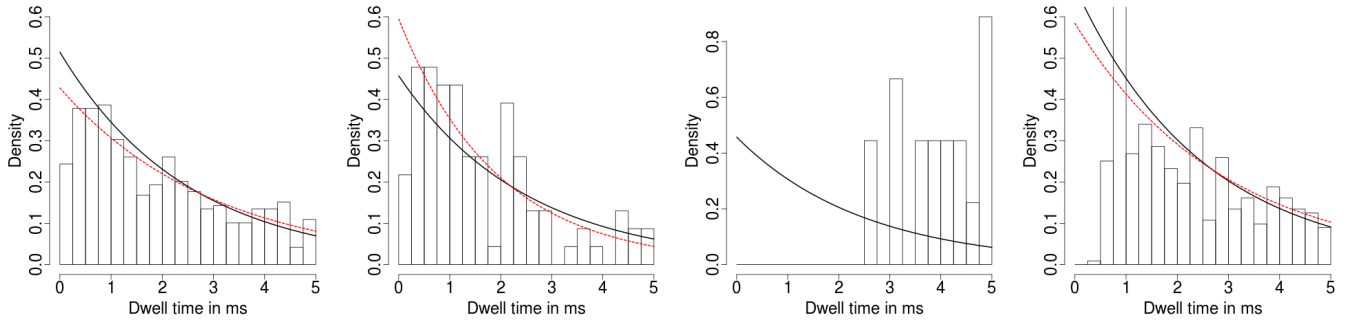

(a) HILDE (b) JULES (c) HSMUCE (d) HMM

Fig. 12. Histograms of the dwell times in the closed state with a length between 0.1 ms and 5 ms to analyze short events, together with the true exponential distribution (—) and exponential fits (.....) that are corrected for missed events. We rescaled all lines such that the area under them are standardized to one to make them comparable to the histograms. This explains why the true distribution does not look always the same. The blue line in the HMM plot indicates an exponential fit when the same missed event correction is used that is applied to the results obtained by HILDE.

We found from Figs. 12 and 13 that HILDE recovers in both cases the exponential distribution very well and estimates both rates of 400 Hz and 20 Hz with 332.59 Hz and 19.2629 Hz accurately. In comparison, JULES is not able to deconvolve all events due to the detection of additional spurious events, compare Fig. 3. The rate for the short events is with 520.16 Hz still accurately, but the rate for the long events is with 9.0682 Hz significantly underestimated. Notably the dwell times are still (almost) exponentially distributed. HSMUCE misses short events, in total it has detected only 18 short events. Hence, a rate for the short events cannot be estimated. The rate for the long events is with 6.0182 Hz underestimated as well. The hidden Markov approach estimated with 347.44 Hz and 19.3949 Hz both rates accurately. However, since this approach misses very short events, for the rate for the short events we had to apply a stricter missed event correction that takes into account only events with a length of at least 0.75 ms. Hence, at least in the used form the hidden Markov approach

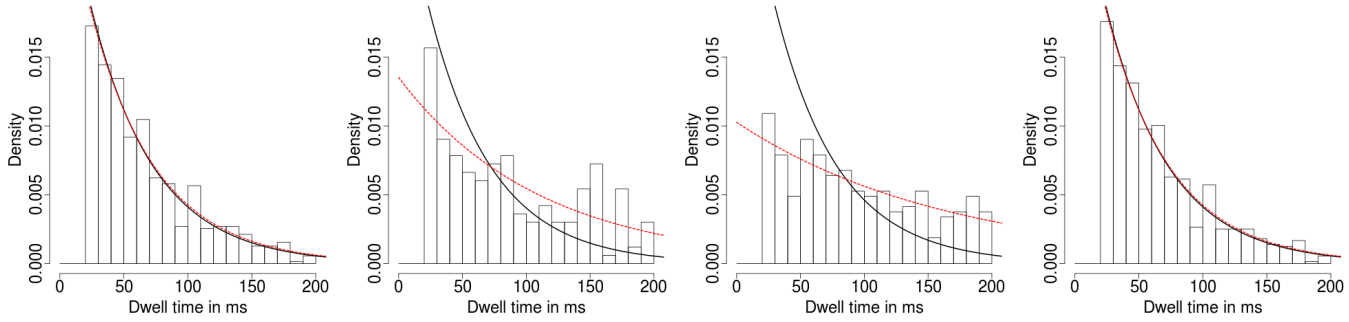

(a) HILDE (b) JULES (c) HSMUCE (d) HMM

Fig. 13. Histograms of the dwell times in the closed state with a length between 20 ms and 200 ms to analyze long events, together with the true exponential distribution (——) and exponential fits (.....) that are corrected for missed events. We rescaled all lines such that the area under them are standardized to one to make them comparable to the histograms. This explains why the true distribution does not look always the same.

is less favorable to analyze short events (since its corrected estimate is based on fewer events and hence will have a larger variance). This is remarkable, since the idealization on very short temporal scales is considered to be a strength of hidden Markov approaches. Finally, the estimated exit probabilities by the Baum-Welch algorithmus of 0.002671 and 0.000644 corresponds to estimated rates of 26.71 Hz and 6.44 Hz which is much worse than the rates estimated using the idealizations obtained by the Viterbi algorithm.

We are now analyzing how often closing events occur. To this end, we analyze the dwell times in the open state or in other words the distance between two closing events. Moreover, we analyze the proportions of short and long events. Therefore, we divide the number of detected events by the estimated probability that such an event is detected assuming an exponential distribution for the dwell times.

We found from Fig. 14 that HILDE, HSMUCE and the hidden Markov approach recover the exponential distribution very well and estimate the rate of 7 Hz with 6.4007 Hz, 6.4919 Hz and 6.2389 Hz accurately. Because of the reasons previously explained, JULES slightly underestimated the rate as 4.3362 Hz. HILDE, JULES and HMM estimated with 0.3608, 0.2982 and 0.4082, respectively, the proportion of short events decently, recall that the truth is $1/3$. This number could not be determined using HSMUCE, since it misses almost all short events. Once again, the Baum-Welch algorithm, with 27.06 Hz and 0.0329, gives much worse results.

All in all, we found that HILDE was indeed able to recover all parameters very well. All other model-free idealization methods had at least one massive problem. The hidden Markov approach might be usable, but requires a more restrictive missed event correction and is also more complicated to apply. One should also keep in mind that we used the true parametric model class as prior knowledge.

E. Robustness

The model we proposed in Section II is a good assumption for ion channel recording at presence of open channel noise. However, in some patch clamp recordings additional high frequency f^2 (violet) and long tailed $1/f$ (pink) noise components have been observed, for a more detailed discussion see [1], [42], [43] and the references therein. Therefore, in this section we examine how robust HILDE is against such noise components. To this end, we revisit the simulation setting from Section IV-B with $s_1 = 10^{-3}$ only.

For the violet noise we use as suggested by [44] a moving average process with coefficients 0.8 and -0.6. For the pink noise we use the algorithm available on *https://github.com/Stenzel/newshadeofpink*. We assume that the pink noise is globally present. More precisely, we reduce the previously present noise by a factor of $1/2$ and add pink noise which is scaled such that its standard deviation is equal to $1/2\sqrt{6.1 \cdot 10^{-5}}$ (half of the standard deviation in the background in Section IV-B). For the high frequency violet noise we consider the setting that the new noise component is state-dependent as well. In other words, we generated errors from such a moving average process and convolved them with the kernel of the lowpass filter instead of assuming white noise errors.

We found in Table V that HILDE is very robust against the additional f^2 but affected by $1/f$ noise. At presence of the latter noise, the standard deviation estimation on the long segments is wrong which causes the detection of false positives in roughly a quarter of the cases. Note, that false positives are caused by the underestimated standard deviation but also by the long range dependency itself. However, the false positives have a small amplitude and therefore do not influence the analysis severely or can be removed by postfiltering. Parameter estimation (not displayed) is slightly effected by $1/f$ noise (estimation of the change-point locations is slightly worse, but estimation of the size of the change is even improved), but not affected by presence of f^2 noise.

V. Data Analysis

A. Measurements

We analyze single channel recordings of PorB from *Neisseria meningitidis* (recall the last paragraph in the introduction). In the following we analyze six traces, each of them is one minute long and consists of 600 000 observations. An example is shown in Fig. 1, which shows distinct heterogeneous noise.

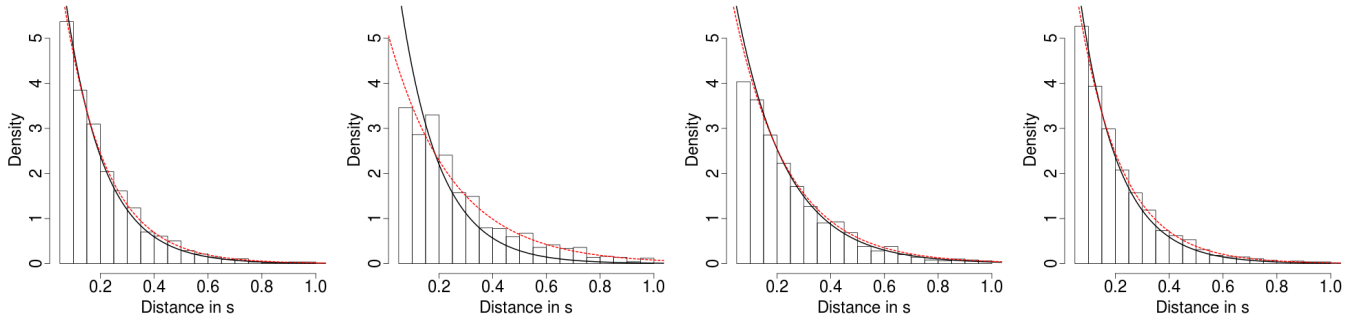

(a) HILDE (b) JULES (c) HSMUCE (d) HMM

Fig. 14. Histograms of the dwell times in the open state, together with the true exponential distribution (——) and exponential fits (.....) that are corrected for missed events. We rescaled all lines such that the area under them are standardized to one to make them comparable to the histograms. This explains why the true distribution does not look always the same.

TABLE V

ROBUSTNESS OF HILDE AGAINST ADDITIONAL NOISE COMPONENTS IN IDEALIZING A SIGNAL WITH AN ISOLATED PEAK HAVING CHANGES AT $\tau_1 = 0.2$ AND $\tau_2 = \tau_1 + \ell/f_s$, $\ell = 2,3,5$, CONDUCTANCE LEVELS $c_0 = c_2 = 0$, $c_1 = 0.32$, VARIANCES $s_0^2 = s_2^2 = 6.1 \cdot 10^{-5}$ AND $s_1^2 = 10^{-3}$. RESULTS ARE BASED ON 10 000 PSEUDO SAMPLES

Noise type	Length (ℓ)	Correctly identified (%)	Detected (%)	False positive (Mean)
White noise	2	99.94	99.98	0.0010
f^2 noise	2	99.94	99.98	0.0010
$1/f$ noise	2	75.04	99.28	0.4351
White noise	3	99.97	100.00	0.0006
f^2 noise	3	99.97	100.00	0.0006
$1/f$ noise	3	75.95	99.32	0.4452
White noise	5	99.95	100.00	0.0010
f^2 noise	5	99.94	100.00	0.0012
$1/f$ noise	5	76.65	99.54	0.4448

Measurements were performed on solvent-free planar bilayers using the Port-a-Patch (Nanion Technologies). Giant unilamellar vesicles (GUVs) composed of 1,2-diphytanoyl-*sn*-glycero-3-phosphocholine (DPhPC)/cholesterol (9:1) were prepared by electroformation (AC, U = 3 V, peak-to-peak, f = 5 Hz, t = 2 h) in the presence of 1 M sucrose at 20 °C. Spreading of a GUV in 1 M KCl, 10 mM HEPES, pH 7.5 on an aperture (d = 1-5 μm) in a borosilicate chip by applying 10-40 mbar negative pressure resulted in a solvent-free membrane with a resistance in the GΩ range. Once the membrane with a GΩ seal was formed, varying amounts of a PorB stock solution (2.2 μM in 200 mM NaCl, 20 mM Tris, 0.1% (w/w) LDAO, pH 7.5) were added to the buffer solution (50 μL) at an applied DC potential of +40 mV. Current traces were recorded at a sampling rate of 10 kHz and filtered with a low-pass four-pole Bessel filter of 1 kHz using an Axopatch 200B amplifier (Axon Instruments). For digitalization, an A/D converter (Digidata 1322; Axon Instruments) was used.

B. Idealization

Idealizations are obtained by HILDE with parameter choices as in Section III-A. Moreover, an illustrative comparison with other approaches was discussed in the introduction (recall Figs. 2—4). In Fig. 1 we see that the channel switches frequently between two conductance levels, roughly between 0.04 nS and 0.36 nS, the variance is roughly $6.1 \cdot 10^{-5}(\text{nS})^2$ in the closed state and $10^{-3}(\text{nS})^2$ in the open state. Moreover, several artifacts seem to be present, see for instance the fluctuating conductance in the open state in the first ten seconds. We stress that such artifacts heavily disturb any idealization that assumes a HMM, confer Fig. 20 in the supplement. Contrarily, the model-free idealization by HILDE (Fig. 5) recovers all visible features on small as well as on large temporal scales accurately. In particular, zooming into single peaks (Fig. 5, lower panels) shows that HILDE fits the observations well which is also a confirmation of our model. Since PorB forms three pores, four different conductance levels are possible. However, in this measurement we see only two different conductance levels. It seems that all three pores open and close simultaneously and we do not observe conductance levels corresponding to only one or two open pores. Such a cooperative opening and closing was observed before as well, see for instance [45].

C. Analysis of Flickering Dynamics

We now use the obtained idealizations to analyze the gating dynamics in a similar fashion as the simulated data in Section IV-D. We will focus in this section on HILDE, but we will compare it in Appendix E in the supplement with analyses based on JULES, HSMUCE and HMM. We say a channel *opens* (a gating event from the lower conductance level to the higher conductance level) if the idealized level is between 0.25 nS and 2 nS and the previous level is between 0 nS and 0.1 nS. To study the amplitude, we consider the conductance difference of all such events. Fig. 15 shows a histogram of the

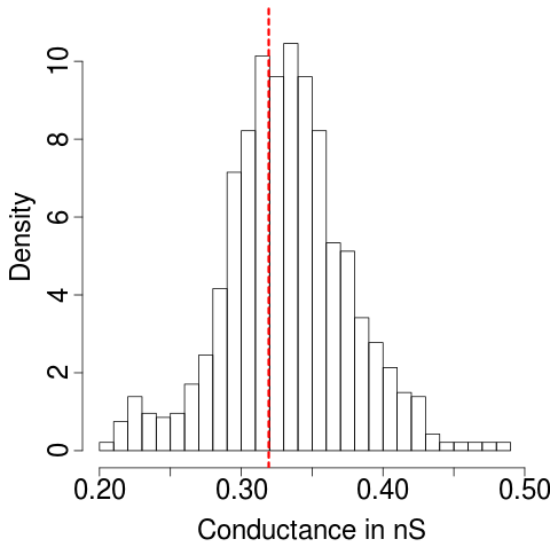

Fig. 15. Histogram of the amplitudes between 0.2 nS and 0.5 nS. (.....) indicates the estimated amplitude of 0.3194 nS by the half sample mode.

so obtained amplitudes between 0.2 nS and 0.5 nS. All other events are either closing events or are considered as artifacts. Such artifacts can for instance be base line fluctuations as discussed in the introduction. We stress that an analysis of the closing events leads to very similar results.

The histogram in Fig. 15 shows only one mode. Hence, all events have the same amplitude up to measurements and idealization errors. This means especially that also the flickering events are full-sized. An amplitude of 0.3194 nS is estimated by the half sample mode [46], computed in `R` by using the *modeest* package. Note that other mode estimators or Gaussian mean estimation lead to similar results. This amplitude coincides with the one obtained by a manual analysis using the pClamp 10.2 software package (Axon Instruments), see [15].

We now analyze the dwell time in the open state and how frequently the channel opens. We take into account events with an amplitude between 0.2 nS and 0.5 nS and with a dwell time between 0.1 ms and 200 ms, since shorter events cannot be detected reliably and longer events are rare and often interrupted by artifacts. Histograms of the dwell time in the open state are shown in Fig. 16 together with an exponential fit using a missed event correction like in [7].

Interestingly, the dwell times do not fit a single exponential distribution, but when we split the events in short (shorter than 5 ms) and long (longer than 20 ms) ones, both fit exponential distributions very well, with an estimated average duration of 51.62 ms and 2.31 ms, respectively. Note, that these estimations are approximations, since an exponential distribution with a large / small rate generates with a small probability a long / short event, but since the average dwell times are very different this error is negligible. Those approximations could have been avoided by fitting phase-type distributions [47, Chapter 2], but missed event corrections for them require more complicated calculations which were not necessary for our data. To best of our knowledge, fast and slow gating at the same time was not observed for PorB before. However, [34] showed that the loop within the pore structure of OmpG leads to fast flickering (fast time constant). If the loop is removed, there is still gating observed but less frequent (slower time constant). Even though this is not the same protein, in PorB we have a loop L3 which is also localized in the pore and forms an α-helix in its center, which constricts the pore to its narrowest point. Hence, our findings support that similar dynamics might occur for PorB as well.

We are now analyzing the distance between two opening events. This is shown in Fig. 17. Moreover, we analyze how many of the openings are short or long. Once again we apply a correction for missed events.

The distance between two events seem to be exponentially distributed and the estimated rate is 5.75 Hz. We found that 39.08% of all opening events were short events. Moreover, we found in Appendix E in the supplement that all results obtained by HILDE could be confirmed by at least one other approach, but none of the other methods was able to reproduce all results obtained by HILDE.

VI. Discussion and Outlook

In this paper we proposed a new model-free idealization method for ion channel recordings, called HILDE. In comparison to existing approaches, HILDE provides still reasonable idealizations under heterogeneous noise, for instance caused by open channel noise. Moreover, it detects and idealizes flickering events reliable, is fully-automatic and can be computed efficiently. It offers great flexibility in adapting to the needs of a specific data analysis by modifying the error probabilities $\alpha = \alpha_1 + \alpha_2$ and the scale $l_{\max}$ that distinguishes short and long events. Its precise idealization is confirmed by simulations and a real data application to PorB recordings. We found that these recordings contain opening events of significantly different length.

We stress that HILDE is modular, i.e., single components like the choice of the test statistics and functionals to optimize can be changed without further modifications. This can be used to adapt HILDE to specific challenges in the measurements. We will discuss several such possibilities in the following. Some of them are implemented in the *clampSeg* package and just require to choose different parameters, for others few lines of code have to be modified.

A. Alternative Approaches

A different underlying interval set can be used for the multiresolution test. The set of all intervals of dyadic length provides in general a good compromise between detection power and computation time. But, if a larger detection power is required, the set of all intervals can be used at the price of a larger computational complexity. The other way around, if faster computation is demanded, a smaller interval set, for instance the dyadic partition like in [33], can be used. This might be particularly beneficial in situations in which the multiresolution test detects almost no events which results in a large computation time. Interesting alternatives are also the

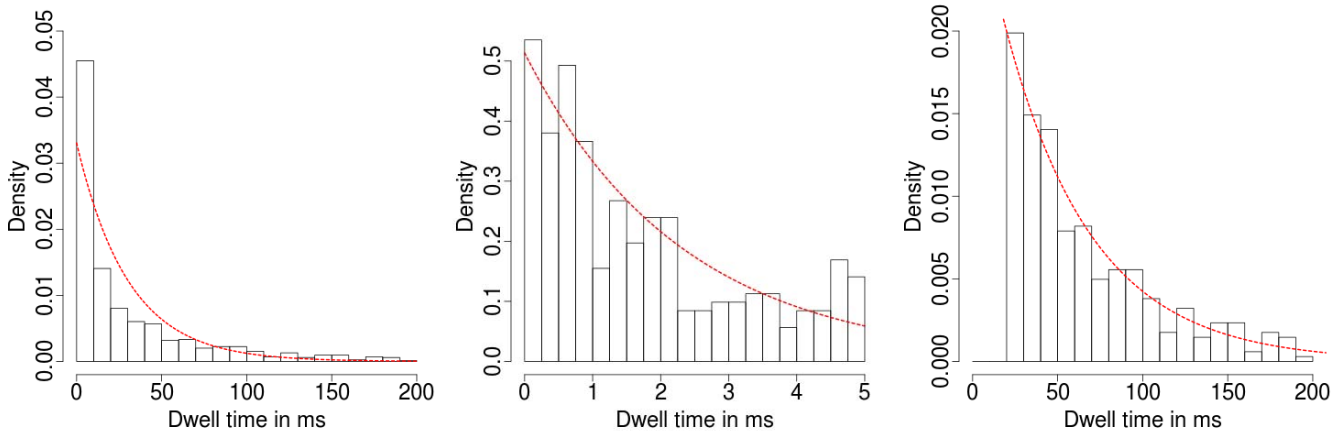

(a) All events between 0.1 ms and 200 ms. (b) Short events between 0.1 ms and 5 ms. (c) Long events between 20 ms and 200 ms.

Fig. 16. Histograms of the dwell times in the open state of all opening events with amplitude between 0.2 nS and 0.5 nS together with exponential fits using a missed event correction (.....).

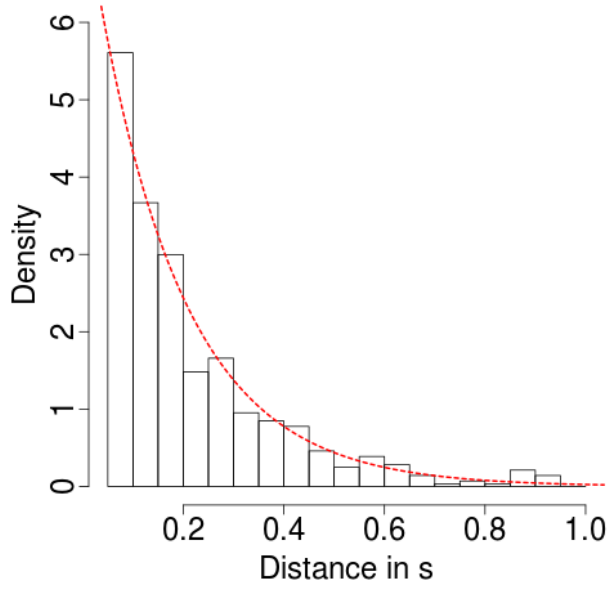

Fig. 17. Histograms of the distances between two opening events with amplitude between 0.2 nS and 0.5 nS together with exponential fits using a missed event correction (.....).

approaches in [48], [49] which require only a slightly larger computational effort than the use of all intervals of dyadic length but detects change-points in a certain sense statistically optimally. A different way to increase the detection power is to use likelihood ratio tests, again at computational expenses. We found in simulations (not displayed) that the likelihood ratio test statistic is slightly more powerful on small scales, but much slower to compute. However, a slightly worse detection power on small scales should not be a big concern, since a refinement by local tests will be done in the next step. Also for detecting events on small scales by local tests, see Section III-C, different statistics can be used to increase the detection power. For instance the likelihood ratio test or maximum likelihood estimators for the parameters (c, s^2) can be considered. However, they are computationally very demanding, since the likelihood function involves the inverse and the determinant of the covariance matrix given by (B.5). Finally, our deconvolution approach assumes still homogeneous noise which we found in simulations works still well at presence of open channel noise, see Tables III and IV. Taking into account the heterogeneous noise might be beneficial, in particular if the noise level differences are large, but difficult, maybe even impossible, since avoiding an ill-conditioned matrix by regularization and keeping the variance levels might be impossible to achieve at the same time.

B. Homogeneous Noise

We designed HILDE particularly to deal with heterogeneous noise. However, taking into account the convolution explicitly when detecting changes is also beneficial if the noise is homogeneous, i.e., a constant variance is assumed. In this situation, its detection power can be further improved by small modifications that utilize the assumption of a constant variance, they are explained in Appendix F in the supplement. We found that HILDE has a better detection power than JULES [7], but at the price of worse separation properties and a larger computation time. More precisely, in the simulations in Section IV-B in [7] we found that JULES is able to detect an isolated peak of length $3.1/f_s$ with probability almost one. In comparison, HILDE requires only $2.3/f_s$ if homogeneous noise is assumed and $2.8/f_s$ if heterogeneous noise is assumed (see Section 3.9.3. in [50]). Remarkably, the detection power of HILDE is even larger than the one of JULES if HILDE does not use the assumption of homogeneous noise which illustrates how much detection power is lost by not taking into account the convolution.

C. Idealizing the Variance

Our focus was on idealizing the conductance while the unknown variance was considered as a nuisance parameter. However, as a byproduct HILDE can easily be extended to

an idealization of the variance which offers for instance a residual analysis of the noise to validate a given model. To this end, we use HILDE to estimate the change-point location of the conductance and assume that these are the change-points of the variance as well. Note that the model of Section II allows the variance to stay constant at such a location but precludes further variance changes. With the definitions from before (see Section III), if a segment is long, the square of the estimator in (B.1) can be used. Afterwards, the variance on short segments can be estimated by the estimator in (B.8). The resulting function will be an idealization of the variance.

Acknowledgment

The authors thank T. Aspelmeier, M. Diehn, B. Eltzner, I. P. Mey, O. M. Schütte, I. Siekmann, I. Tecuapetla-Gómez, and F. Werner for fruitful discussions. They also thank two anonymous referees for their helpful comments and suggestions which helped us to improve this paper.

References

[1] E. Neher and B. Sakmann, "Single-channel currents recorded from membrane of denervated frog muscle fibres," *Nature*, vol. 260, no. 5554, pp. 799–802, Apr. 1976.

[2] B. Sakmann and E. Neher, *Single-Channel Recording*, 2nd ed. New York, NY, USA: Springer, 1995.

[3] R. S. Kass, "The channelopathies: Novel insights into molecular and genetic mechanisms of human disease," *J. Clin. Invest.*, vol. 115, no. 8, pp. 1986–1989, Aug. 2005.

[4] J. P. Overington, B. Al-Lazikani, and A. L. Hopkins, "How many drug targets are there?" *Nature Rev. Drug Discovery*, vol. 5, no. 12, pp. 993–996, Dec. 2006.

[5] D. Colquhoun, *Practical Analysis of Single Channel Records* (Microelectrode Techiques. The Plymouth Workshop Handbook). Cambridge, U.K.: Company of Biologists, 1987.

[6] T. Hotz *et al.*, "Idealizing ion channel recordings by a jump segmentation multiresolution filter," *IEEE Trans. Nanobiosci.*, vol. 12, no. 4, pp. 376–386, Dec. 2013.

[7] F. Pein, I. Tecuapetla-Gómez, O. M. Schütte, C. Steinem, and A. Munk, "Fully automatic multiresolution idealization for filtered ion channel recordings: Flickering event detection," *IEEE Trans. Nanobiosci.*, vol. 17, no. 3, pp. 300–320, Jul. 2018.

[8] F. J. Sigworth, "Open channel noise. I. Noise in acetylcholine receptor currents suggests conformational fluctuations," *Biophys. J.*, vol. 47, no. 5, pp. 709–720, May 1985.

[9] F. J. Sigworth, "Open channel noise. II. A test for coupling between current fluctuations and conformational transitions in the acetylcholine receptor," *Biophys. J.*, vol. 49, no. 5, pp. 1041–1046, May 1986.

[10] F. J. Sigworth, D. W. Urry, and K. U. Prasad, "Open channel noise. III. High-resolution recordings show rapid current fluctuations in gramicidin A and four chemical analogues," *Biophys. J.*, vol. 52, no. 6, pp. 1055–1064, Dec. 1987.

[11] S. H. Heinemann and F. J. Sigworth, "Open channel noise. IV. Estimation of rapid kinetics of formamide block in gramicidin A channels," *Biophys. J.*, vol. 54, no. 4, pp. 757–764, Oct. 1988.

[12] S. H. Heinemann and F. J. Sigworth, "Open channel noise. V. Fluctuating barriers to ion entry in gramicidin A channels," *Biophys. J.*, vol. 57, no. 3, pp. 499–514, Mar. 1990.

[13] S. H. Heinemann and F. J. Sigworth, "Open channel noise. VI. Analysis of amplitude histograms to determine rapid kinetic parameters," *Biophys. J.*, vol. 60, no. 3, pp. 577–587, Sep. 1991.

[14] M. Virji, "Pathogenic neisseriae: Surface modulation, pathogenesis and infection control," *Nat. Rev. Microbiol.*, vol. 7, no. 4, p. 274, 2009.

[15] A. Bartsch *et al.*, "High-resolution experimental and computational electrophysiology reveals weak β-lactam binding events in the porin porB," *Sci. Rep.*, vol. 9, no. 1, 2019, Art. no. 1264.

[16] A. M. VanDongen, "A new algorithm for idealizing single ion channel data containing multiple unknown conductance levels," *Biophys. J.*, vol. 70, no. 3, pp. 1303–1315, Mar. 1996.

[17] R. Gnanasambandam, M. S. Nielsen, C. Nicolai, F. Sachs, J. P. Hofgaard, and J. K. Dreyer, "Unsupervised idealization of ion channel recordings by minimum description length: Application to human PIEZO1-channels," *Frontiers Neuroinform.*, vol. 11, p. 31, Apr. 2017.

[18] F. G. Ball and J. A. Rice, "Stochastic models for ion channels: Introduction and bibliography," *Math. Biosci.*, vol. 112, no. 2, pp. 189–206, Dec. 1992.

[19] L. Venkataramanan, R. Kuc, and F. J. Sigworth, "Identification of hidden Markov models for ion channel currents. III. Bandlimited, sampled data," *IEEE Trans. Signal Process.*, vol. 48, no. 2, pp. 376–385, Feb. 2000.

[20] F. Qin, A. Auerbach, and F. Sachs, "Hidden Markov modeling for single channel kinetics with filtering and correlated noise," *Biophys. J.*, vol. 79, no. 4, pp. 1928–1944, Oct. 2000.

[21] M. C. M. de Gunst, H. R. Künsch, and J. G. Schouten, "Statistical analysis of ion channel data using hidden Markov models with correlated state-dependent noise and filtering," *J. Amer. Stat. Assoc.*, vol. 96, no. 455, pp. 805–815, Sep. 2001.

[22] I. Siekmann *et al.*, "MCMC estimation of Markov models for ion channels," *Biophys. J.*, vol. 100, no. 8, pp. 1919–1929, Apr. 2011.

[23] M. Diehn, A. Munk, and D. Rudolf, "Maximum likelihood estimation in hidden Markov models with inhomogeneous noise," *ESAIM, Probab. Statist.*, vol. 23, pp. 492–523, Apr. 2019.

[24] G. Yellen, "Ionic permeation and blockade in Ca2+-activated K+ channels of bovine chromaffin cells," *J. Gen. Physiol.*, vol. 84, no. 2, pp. 157–186, Aug. 1984.

[25] I. Schroeder, "How to resolve microsecond current fluctuations in single ion channels: The power of beta distributions," *Channels*, vol. 9, no. 5, pp. 262–280, Sep. 2015.

[26] A. J. W. Hartel, S. Shekar, P. Ong, I. Schroeder, G. Thiel, and K. L. Shepard, "High bandwidth approaches in nanopore and ion channel recordings—A tutorial review," *Anal. Chim. Acta*, vol. 1061, pp. 13–27, Jul. 2019.

[27] A. Viterbi, "Error bounds for convolutional codes and an asymptotically optimum decoding algorithm," *IEEE Trans. Inf. Theory*, vol. IT-13, no. 2, pp. 260–269, Apr. 1967.

[28] A. Fuliński, Z. Grzywna, I. Mellor, Z. Siwy, and P. N. R. Usherwood, "Non-Markovian character of ionic current fluctuations in membrane channels," *Phys. Rev. E, Stat. Phys. Plasmas Fluids Relat. Interdiscip. Top.*, vol. 58, no. 1, pp. 919–924, Jul. 1998.

[29] I. Goychuk, P. Hänggi, J. L. Vega, and S. Miret-Artés, "Non-Markovian stochastic resonance: Three-state model of ion channel gating," *Phys. Rev. E, Stat. Phys. Plasmas Fluids Relat. Interdiscip. Top.*, vol. 71, no. 6, Jun. 2005, Art. no. 061906.

[30] S. Mercik and K. Weron, "Stochastic origins of the long-range correlations of ionic current fluctuations in membrane channels," *Phys. Rev. E, Stat. Phys. Plasmas Fluids Relat. Interdiscip. Top.*, vol. 63, no. 5, Apr. 2001, Art. no. 051910.

[31] C. Shelley, X. Niu, Y. Geng, and K. L. Magleby, "Coupling and cooperativity in voltage activation of a limited-state BK channel gating in saturating Ca2+," *J. Gen. Physiol.*, vol. 135, no. 5, pp. 461–480, May 2010.

[32] K. Frick, A. Munk, and H. Sieling, "Multiscale change point inference (with discussion and rejoinder by the authors)," *J. R. Statist. Soc. B*, vol. 76, no. 3, pp. 495–580, 2014.

[33] F. Pein, H. Sieling, and A. Munk, "Heterogeneous change point inference," *J. Roy. Stat. Soc., B, Stat. Methodol.*, vol. 79, no. 4, pp. 1207–1227, Sep. 2017.

[34] W. Grosse *et al.*, "Structure-based engineering of a minimal porin reveals loop-independent channel closure," *Biochemistry*, vol. 53, no. 29, pp. 4826–4838, Jul. 2014.

[35] P. R. Singh, M. Ceccarelli, M. Lovelle, M. Winterhalter, and K. R. Mahendran, "Antibiotic permeation across the OmpF channel: Modulation of the affinity site in the presence of magnesium," *J. Phys. Chem. B*, vol. 116, no. 15, pp. 4433–4438, Apr. 2012.

[36] F. Pein, T. Hotz, I. Tecuapetla-Gómez, and T. Aspelmeier. (2019). *clampSeg: Idealisation of Patch Clamp Recordings R Package Version 1.1-0*. [Online]. Available: https://CRAN.R-project.org/package=clampSeg

[37] I. Tecuapetla-Gómez and A. Munk, "Autocovariance estimation in regression with a discontinuous signal and m-dependent errors: A difference-based approach," *Scand. J. Stat.*, vol. 44, no. 2, pp. 346–368, 2017.

[38] R. Killick, P. Fearnhead, and I. A. Eckley, "Optimal detection of changepoints with a linear computational cost," *J. Amer. Stat. Assoc.*, vol. 107, no. 500, pp. 1590–1598, Dec. 2012.

[39] H. Li, A. Munk, and H. Sieling, "FDR-control in multiscale change-point segmentation," *Electron. J. Statist.*, vol. 10, no. 1, pp. 918–959, 2016.

[40] R. Maidstone, T. Hocking, G. Rigaill, and P. Fearnhead, "On optimal multiple changepoint algorithms for large data," *Statist. Comput.*, vol. 27, no. 2, pp. 519–533, Mar. 2017.

[41] M. Diehn, "Inference in inhomogeneous hidden Markov models with application to ion channel data," Ph.D. dissertation, Inst. Math. Stochastics, Georg-August-Univ. Göttingen, Göttingen, Germany, 2017. [Online]. Available: http://hdl.handle.net/11858/00-1735-0000-0023-3FB4-2

[42] L. Venkataramanan, J. L. Walsh, R. Kuc, and F. J. Sigworth, "Identification of hidden Markov models for ion channel currents. I. Colored background noise," *IEEE Trans. Signal Process.*, vol. 46, no. 7, pp. 1901–1915, Jul. 1998.

[43] R. A. Levis and J. L. Rae, "The use of quartz patch pipettes for low noise single channel recording," *Biophys. J.*, vol. 65, no. 4, pp. 1666–1677, Oct. 1993.

[44] L. Venkataramanan, R. Kuc, and F. J. Sigworth, "Identification of hidden Markov models for ion channel currents. II. State-dependent excess noise," *IEEE Trans. Signal Process.*, vol. 46, no. 7, pp. 1916–1929, Jul. 1998.

[45] J. Song, C. A. S. A. Minetti, M. S. Blake, and M. Colombini, "Successful recovery of the normal electrophysiological properties of PorB (class 3) porin from *Neisseria meningitidis* after expression in *Escherichia coli* and renaturation," *Biochimica et Biophysica Acta (BBA)-Biomembranes*, vol. 1370, no. 2, pp. 289–298, Mar. 1998.

[46] T. Robertson and J. D. Cryer, "An iterative procedure for estimating the mode," *J. Amer. Stat. Assoc.*, vol. 69, no. 348, pp. 1012–1016, Dec. 1974.

[47] M. F. Neuts, *Matrix-Geometric Solutions in Stochastic Models: An Algorithmic Approach*. Chelmsford, MA, USA: Courier Corporation, 1994.

[48] H. P. Chan and G. Walther, "Detection with the scan and the average likelihood ratio," *Statistica Sinica*, vol. 23, no. 1, pp. 409–428, Jan. 2013.

[49] S. Kovács, H. Li, P. Bühlmann, and A. Munk, "Seeded binary segmentation: A general methodology for fast and optimal change point detection," 2020, *arXiv:2002.06633*. [Online]. Available: http://arxiv.org/abs/2002.06633

[50] F. Pein, "Heterogeneous multiscale change-point inference and its application to ion channel recordings," Ph.D. dissertation, Georg-August-Univ. Göttingen, Göttingen, Germany, 2017. [Online]. Available: http://hdl.handle.net/11858/00-1735-0000-002E-E34A-7.

[51] F. Pein, T. Hotz, H. Sieling, and T. Aspelmeier. (2019). *stepR: Multiscale Change-Point Inference R Package Version 2.1-0*. [Online]. Available: https://CRAN.R-project.org/package=stepR

[52] F. Enikeeva, A. Munk, and F. Werner, "Bump detection in heterogeneous Gaussian regression," *Bernoulli*, vol. 24, no. 2, pp. 1266–1306, May 2018.

[53] A. B. Olshen, E. S. Venkatraman, R. Lucito, and M. Wigler, "Circular binary segmentation for the analysis of array-based DNA copy number data," *Biostatistics*, vol. 5, no. 4, pp. 557–572, Oct. 2004.